LBNL-59921

Energy flow in a hadronic cascade: Application to hadron calorimetry

Donald E. Groom

Lawrence Berkeley National Laboratory, Berkeley, CA 94720

Abstract

The hadronic cascade description developed in an earlier paper is extended to the response of an idealized fine-sampling hadron calorimeter. Calorimeter response is largely determined by the transfer of energy E_e from the hadronic to the electromagnetic sector via π^0 production. Fluctuations in this quantity produce the "constant term" in hadron calorimeter resolution. The increase of its fractional mean, $f^0_{\rm em} = \langle E_e \rangle / E$, with increasing incident energy E causes the energy dependence of the π/e ratio in a noncompensating calorimeter. The mean hadronic energy fraction, $f^0_h = 1 - f^0_{\rm em}$, was shown to scale very nearly as a power law in E: $f^0_h = (E/E_0)^{m-1}$, where $E_0 \approx 1$ GeV for pions, and $m \approx 0.83$. It follows that $\pi/e = 1-(1-h/e)(E/E_0)^{m-1}$, where electromagnetic and hadronic energy deposits are detected with efficiencies e and h, respectively. Fluctuations in these quantities, along with sampling fluctuations, are incorporated to give an overall understanding of resolution, which is different from the usual treatments in interesting ways. The conceptual framework is also extended to the response to jets and the difference between π and p response.

1 Introduction

In Paper I[1] we developed a conceptual basis for understanding the division between hadronic and electromagnetic energy deposition in a contained hadronic cascade.[1] The model "calorimeter" was a very large lead or iron cylinder, with no energy leakage except via muons, neutrinos, and front-surface albedo losses. Extensive Monte Carlo simulations gave results in good agreement with test-beam measurements. The relevant conclusions of the paper were that:

[1] Most of the content of Paper I was first presented at the 1989 Workshop on Calorimetry for the Superconducting Super Collider[2].

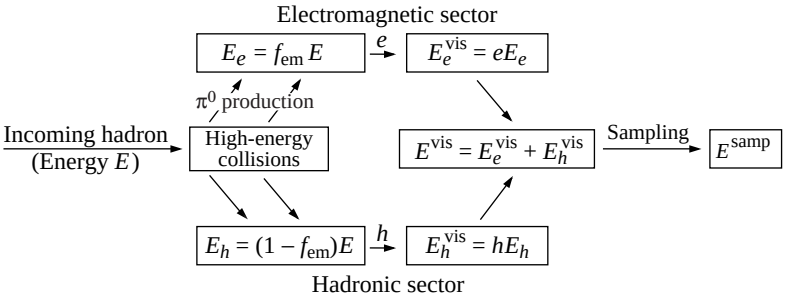

Fig. 1. Energy flow in a hadronic cascade. A fraction $f_{\rm em}$ (with energy-dependent mean $f_{\rm em}^0$) is transferred to the electromagnetic sector through π^0 production in repeated hadronic inelastic collisions. The em and hadronic energy deposits after the division are separately stochastic, and so must be treated as parallel processes. Each produces a visible signal, whose sum $E^{\rm vis}$ is observed. EFlow_simple

(1) All significant hadronic energy deposition is by low-energy particles ($\lesssim$1 GeV), whose energy and species distribution in a given medium is independent of the energy or species of the incident hadron. (Hadronic energy is defined as all energy not carried away by π^0 decay photons.[2]) The existence of this "universal low-energy hadron spectrum" makes it possible to define an energy-independent efficiency h for the conversion of this energy into a visible signal in a fine-sampling calorimeter.

(2) In each high-energy collision of the hadronic cascade, a significant fraction (typically 1/4) of the energy is transferred to the electromagnetic (em) sector via π^0 production. A sequence of high-energy hadronic collisions bleeds off a larger and larger fraction of the energy as the incident energy E increases. The net fraction transferred to the em sector is $f_{\rm em}$, and the mean em fraction is $f_{\rm em}^0$. This one-way flow is illustrated in Fig. 1.[3]

(3) In particular, the mean fraction of the energy $f_h = 1 - f_{\rm em}$ in the hadronic sector scales very nearly as a power of the incident energy,

$$f_h^0(E) \equiv \langle f_h(E) \rangle = (E/E_0)^{m-1} \ , \tag{1}$$

where $m \approx 0.83$ (with some mild absorber Z dependence) and $E_0 \approx 1$ GeV for pions and ≈ 2.6 GeV for protons. Physically, m is related to the mean number of secondaries and the mean energy fraction going into π^0's in any given collision in the cascade, and E_0 is the energy at which multiple pion production becomes significant.

(4) It was predicted that a calorimeter would have a different response to a proton than to an electron.

[2] Assigning nuclear gamma ray energy to the hadronic sector is an awkward but necessary feature of the model, since its contribution scales with the hadronic fraction. This point is discussed further in Sec. 6.

[3] Wigmans observes that the actual number of π^0's produced is quite small[3].

The observations pertain equally well to a homogeneous or fine-sampling calorimeter, and have significant implications for its response and resolution. "Fine-sampling" means that absorber and sensor elements are thin compared to both the em radiation length and the neutron interaction length. It has the same structure throughout: no separate em compartment or rear catcher. It can be an inorganic crystal calorimeter, a uranium/liquid argon calorimeter, or a lead/scintillator-fiber calorimeter.

The power-law *approximation* given in Eq. (1) is just that, for reasons discussed in Paper I . It seems to work well over the energy range of available test-beam data, about 10 GeV to 375 GeV, and it has the required asymptotic properties: It is everywhere positive, and $f_h^0 \to 0$ $(\pi/e \to 1)$ as $E \to \infty$. The physical assumptions it is based upon become less dependable at very high energies and are not valid at energies below the threshold for multiple pion production.

As far as possible, results in this paper are obtained without recourse the the powerlaw approximation for f_h^0, to obtain more general results than those relying on this more approximate form.

Most of the results reported in this paper were first reported at a variety of calorimetry conferences and appear in the various *Proceedings* [2,4–9]. The Monte Carlo results used in these papers are often based on now-superseded versions of hadronic cascade simulation codes[10], the oldest being FLUKA86. In particular, nuclear gamma rays were not included, so that the em deposit is exclusively via π^0 production. Since these versions many improvements in the codes have been made, e.g., improvements in FLUKA by Ferrari and Sala[11], especially in the nuclear physics modeling. The failings of the old code are apparent in Fig. 2(b), for example, where the points fall below the 45° line because of unscored hadronic energy. A large fraction of the unscored energy is evidently that of nuclear gamma rays. On the other hand, electromagnetic energy deposition was very well described[12] and can be trusted. In Paper I we reported simulations with MARS10, HETC, and FLUKA, which, though based on different high-energy interaction models, were in excellent agreement. Since in this paper I depend *only* upon the high-energy division between the em and hadronic sectors, calculations based on the older code have not been repeated.

Recent developments are incorporated, some of which were predicted or discussed in Paper I. These include Cherenkov readout[13], which is for the most part sensitive only to the em energy deposition, and observation of the π/p response difference[14].

Central to the paper is the discussion of resolution, where conditional probability distributions (p.d.f.'s) are combined to account for parallel, independent

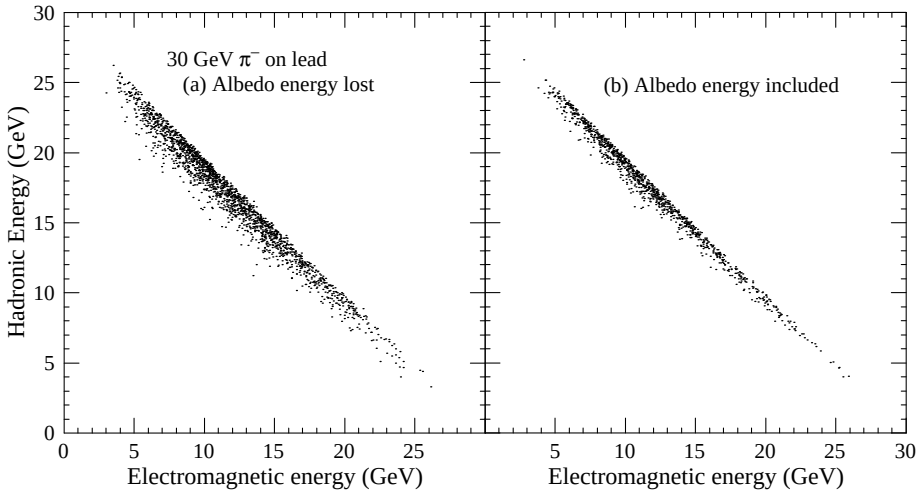

Fig. 2. Calculated energy deposit distributions for 30 GeV negative pions incident on a lead "calorimeter." In case (a) backscattered energy is lost; in (b) it is retained. comp30_bothdot_h

stochastic processes.

Hadron calorimetry is a well-traveled road, explored in hundreds, if not thousands, of papers over several decades. The object here is to present a broad-brush treatment of hadronic cascades in a simplified generic calorimeter, in hopes that a somewhat nonstandard approach can contribute to our physical understanding of a real calorimeter. Real calorimeters, with front em compartments, rear catchers, leakage, crack corrections, jet finding algorithms, and a myriad of other problems, are described in dozens of test-beam study results, as well as in published studies of compensation, the role of neutrons, and other matters. These are discussed in detail in Wigmans' book[3] and review[15] , the review by Leroy and Rancoita[16], and in their many citations. None of these practical problems are discussed here.

2 Albedo and f_{em}

The em fraction $f_{\mathrm{em}} = E_e/E$ increases with energy, but at any given energy it is subject to large fluctuations. FLUKA simulations of the em/hadronic energy division are shown in Fig. 2. The model absorber consisted of a large lead cylinder (50 cm radius, 250 cm long) in which the first 25 cm (about 1.5 interaction lengths) was treated as a separate region. In Fig 2(a) no distinction is made between the regions, while in 2(b) interaction of the incident pion was not permitted in the front section, but energy deposited there is included. It acted as a catcher for back-scattered interaction debris. The distribution about the ideal $E_h = 1 - E_{\mathrm{em}}$ shows less scatter in 2(b) because front-face, or albedo, losses are included. Most albedo loss comes from backward or backscattered

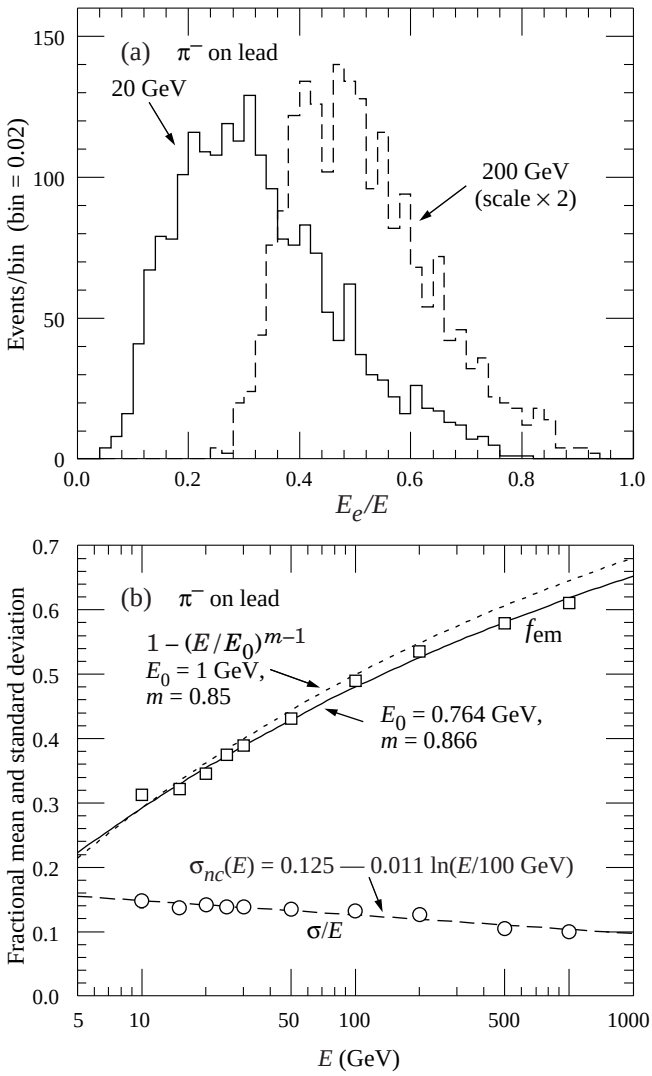

Fig. 3. FLUKA simulations for negative pions incident on a lead "calorimeter." (a) Distribution of the fractional mean em ($\equiv \pi^0$) energy deposit for 20 and 200 GeV incident pions, and (b) energy dependence of the mean and standard deviation. f0_distr

products of the first collision; when the first interaction occurs deep in the detector there is essentially no albedo loss. Runs at 50 GeV with and without an "albedo catcher" show an average difference in deposited energy is 0.43 GeV, or 0.8%. Out of 1000 cascades 50% lost less than 0.2 GeV, and 3.4% lost more than 2 GeV. In the simulations the amount of lost albedo energy rises only slowly with increasing incident energy, as might be expected. While these losses are not totally negligible, I omit them from resolution consideration in Sec, 7 because (a) the distribution is sharply peaked at near-zero loss, and (b) the losses are small, particularly at higher energies.

For reasons discussed in the introduction, the points shown in Fig. 2 scatter below the 45° line because older versions of FLUKA did not account for all of

the hadronic energy deposit, even in the absence of albedo losses. Presumably most of this downward scatter (about 15% in the worst case) is the result of the program's failure to tally nuclear gamma rays, mostly the result of slow neutron capture by nuclei. According to Ferrari and Sala[18], these might account for nearly 10% (Fe) or 20% (Pb) of the $\pi^0 + \gamma$ fraction, or 5%–10% of the total energy deposit. This energy fraction is not counted as part of what I call visible em deposit, since the it scales with the hadronic fraction, not the π^0 fraction. Given that the hadronic fraction is underestimated, it is better to take the hadronic fraction as

$$f_h \equiv 1 - f_{\rm em}, \text{ or } E_h \equiv E - E_{\rm em} \ . \tag{2}$$

As the number of Monte Carlo events in the sample increases, the (E_h, E_e) distribution projected onto the E_e axis approaches the marginal distribution $\Pi(E_e)$, the p.d.f for the em energy. Two FLUKA-generated (unnormalized) examples of E_e/E distributions are shown in Fig. 3(a). The mean and standard deviations are shown in Fig. 3(b). The fractional mean $\langle E_e/E \rangle$ moves to the right with increasing energy, and can be represented by $f^0_{\rm em} = 1 - (E/E_0)^{m-1}$. The rms width of E_e/E distribution, σ_{nc}, is remarkably constant, with only a 40% decrease over two orders of magnitude in energy. This likely occurs because of the slow logarithmic growth of multiplicity. The dimensionless "coefficient of skewness," $\gamma_1 = \mu_3/(\sigma^3_{nc} E^3)$ (where μ_3 is the third moment about the mean), is constant to within the Monte Carlo statistics with a value near 0.6. There are no significant higher moments within the sensitivity of the simulations.

It is to be expected that different or better cascade simulations would result in a somewhat different shape and different moments. What is of consequence here is that a function $\Pi(E_{\rm em})$ exists which describes the energy distribution of the π^0's for a given primary energy E; no significant conclusions depend upon the details.

It is possible to understand the contribution of $\Pi(E_{\rm em})$ to the calorimeter resolution by a geometrical construction. Figure 4 shows the same MC "events" as Fig. 2(b), but with the lost hadronic energy restored as per Eq. (2) (except for some vertical scatter retained for clarity). The observed energy distribution in the absence of sampling fluctuations is the projection of this distribution onto a diagonal line at $\theta = \tan^{-1}(h/e)$. The projection of the limiting cases ($f_{\rm em} = 0$ and $f_{\rm em} = 1$) are shown by the arrows. All of the events thus project onto the solid part of the line, with length $|\cos\theta - \sin\theta| = (1 - h/e)\cos\theta$. The sampled $\Pi(E_{\rm em})$ distribution in Fig. 3(b) is replotted as the gray histogram along the $E_{\rm em}/E$ axis. A point at $E_{\rm em}/E = 1$ projects to the end of the solid segment, so the energy scale along this axis is foreshortened by $\cos\theta$. The solid line segment, rescaled by $1/\cos\theta$, is $(1 - h/e)$ long. The nearly-constant fractional standard deviation of $\Pi(E_{\rm em}/E)$, σ_{nc}, also scales as $(1 - h/e)$. It

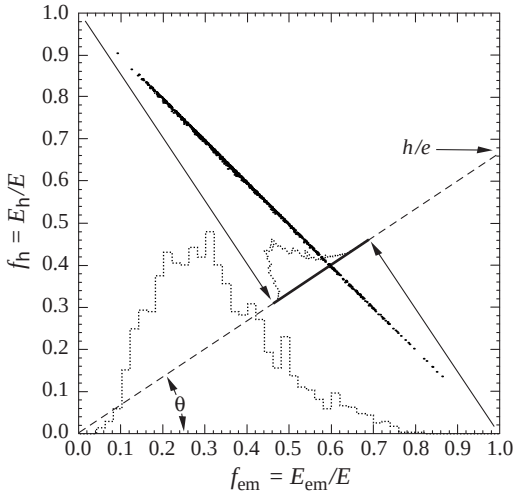

Fig. 4. The projection of "events" onto the diagonal line at $\theta = \tan^{-1}(h/e)$ gives the energy distribution for a calorimeter in the absence of any other fluctuations. Events must fall along the solid segment. One can imagine the projection as θ increases from 0° ($h/e = 0$, large dotted histogram) to 45° ($h/e = 1$, full compensation), where it approaches a δ-function. compf30_corr_scat

thus contributes $(1 - h/e)\sigma_{nc}$ (in quadrature) to the calorimeter resolution.

3 π/e

An electromagnetic shower initiated by an electron or π^0-decay photons produces a visible signal (potentially observable via ionization or Cherenkov light) in a calorimeter with efficiency e. Most of the ionization is by electrons and positrons with energies below the critical energy, of order 10 MeV (21.8 MeV for iron, 7.0 MeV for uranium). The response, here temporarily called "e," is usually linear in the incident energy E, and so serves to calibrate the energy scale:

$$\text{“}e\text{”} = e\,E \tag{3}$$

As shown in Paper I, the visible signal produced by hadron interactions also comes predominately from low-energy ionizing particles whose spectra and relative abundance are independent of the incident hadron energy. Many mechanisms are at play, including endothermic nuclear spallation. Neutrons play an especially significant role[17]. These mechanisms are exhaustively treated in the literature; for example, in Refs. [3,15,16,18]. The sum of all the hadronic energy deposit mechanisms (excluding showers by π^0 decay photons) produces

an observable signal with efficiency h. In most cases $h/e \leq 1$.[4] For a mean hadronic fraction $f_h^0 = 1 - f_{\rm em}^0$,

$$\begin{aligned} \text{“}\pi\text{”} = &\quad e\, f_{\rm em}^0 E + h\, f_h^0 E \\ &= eE[1 - (1 - h/e) f_h^0] \ . \end{aligned} \tag{4}$$

In the case of an an incident pion, the response relative to an electron is

$$\pi/e = 1 - (1 - h/e) f_h^0 \ . \tag{5}$$

Specializing to our powerlaw form for f_h^0,

$$\pi/e = 1 - (1 - h/e)(E/E_0)^{m-1} \equiv 1 - aE^{m-1} \ , \tag{6}$$

where, as above, $m \approx 0.82$ to 0.86. (π/e is only defined for an ensemble of events, so it is implicitly a mean value.) Since the physics leading to the powerlaw involves a multistep cascade, it is not expected to be dependable below 5–10 GeV. Only $a = (1 - h/e)E_0^{1-m}$ can be obtained from fits to data, at least in a single-readout calorimeter. The exponent m should be fitted as well, but it is not as well-determined. For incident pions (not protons) a range of E_0's near 1 GeV fit equally well because it is raised to a small power. *The ratio h/e cannot be obtained from a measurement of π/e as a function of energy without other information or some assumption about E_0.*

I emphasize that my powerlaw representation is not empirical, but follows from an induction argument. It has the correct asymptotic limit, since $f_{\rm em} \to 1$ as $E \to \infty$. For a 10^{19} eV proton-induced air shower, for example, $f_{\rm em} \approx 0.98$, in accord with the usual cosmic ray expectation and observation that nearly all the energy deposit at very high energies is electromagnetic.[5] The expected behavior of π/e is shown in Fig. 5.

Representative fits of test-beam results to Eq. (6) are shown in Fig. 6. Solid curved are least-squares fits with both m and a allowed to vary, while m is constrained to its nominal value for the fits shown as dashed lines. In the case of the copper/quartz-fiber calorimeter, an additional fit (dotted line) is made with $a = 0.90$, my *a priori* expectation for such a calorimeter.

Given fits wide range of experimental data which has been fitted to test the powerlaw, one suspects that the disparate results (e.g. the high value of m for the CDF end-plug calorimeter) indicate data reduction problems. The low

[4] A remarkable exception is provided by the WA 78 calorimeter[19].

[5] This is an illustrative example only, because there is no expectation that m will remain even relatively constant over such a large energy range.

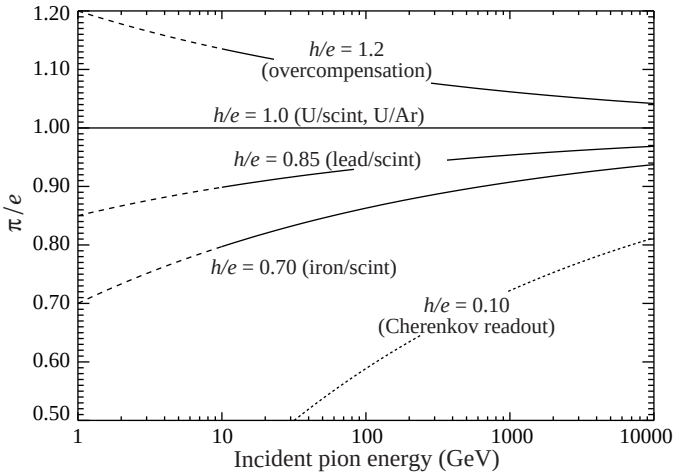

Fig. 5. Energy dependence of π/e expected for several values of h/e with the assumption that $E_0 = 1$ GeV. For almost all calorimeters, $h/e < 1$. The lower dotted line, for $h/e \ll 1$, should be applicable to a calorimeter with Cherenkov detector readout; experimentally, it turns out to be ≈ 0.25[13]. The powerlaw description is not expected to be dependable below about 10 GeV, but nonetheless seems adequate at 5 GeV. pie_theory

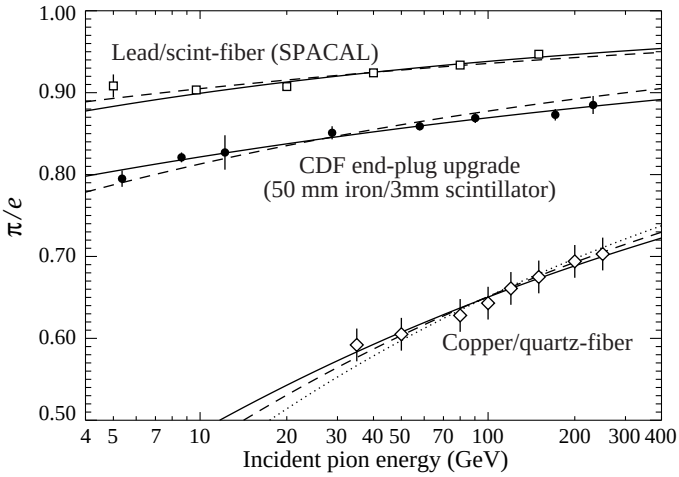

Fig. 6. Fits to test-beam results for a lead/scintillator-fiber)[20], for the CDF upgrade end-cap hadron calorimeter (50 mm iron/3 mm scintillator sheets)[21], and for a copper/quartz-fiber test calorimeter[13]. Fit parameters are given in Table 1. datafits_pie

value of a (high value of h/e) for the copper/quartz-fiber calorimeter is not understood in the context of the present analysis. Since the threshold energy for electrons in silica is close to 1 MeV, it is hard to imagine that electrons Compton-scattered by nuclear gamma rays contribute much.

Table 1
Powerlaw fits to a variety of π/e measurements. The ZEUS uranium/scintillator[22] and D0 uranium/argon[23] calorimeters are so close to compensating as to be uninteresting in this context.

Calorimeter	m	a	χ^2	h/e*	Expected h/e
SPACAL[20]	0.788	0.164	9.2	0.836	0.853–0.895†
(lead/scint-fiber)	*0.830*‡	0.141	14.0	0.859	0.853–0.895†
CDF end-plug had cal[21]	0.865	0.244	2.7	0.756	0.667†
(50 mm Fe/3 mm scint)	*0.816*‡	0.286	14.1	0.714	0.667†
Copper/quartz-fiber[13]	0.833	0.753	2.6	0.247	0.05 to 0.15§
(QFCAL)	*0.816*‡	0.814	3.8	0.186	0.05 to 0.15§
	0.794	*0.900*¶	8.9	*0.100*¶	0.05 to 0.15§

*Assuming $E_0 = 1$ GeV.

† Paper I, Table 1. (The calorimeters have only approximately the same structure.)

‡ Dashed curves in Fig. 6: m held fixed at the value given by the fitted line in Paper I, Fig. 12. Error in m from this work is ± 0.01 to ± 0.015.

§ Perhaps 5% of the total energy ($\approx$ 10% of the hadronic energy) is deposited via ionization by Compton-scattered electrons from several-MeV nuclear gamma rays, mostly in the Cu absorber. Some of them produce Cherenkov radiation over part of their range in the quartz fibers. A small fraction ($\sim$ 3%?) of the hadronic energy is deposited via ionization by high-energy pions, which can also produce Cherenkov light. It is difficult to imagine how h/e can be as great as 0.10, but fits to the data yield 0.20–0.25.

¶ Dotted curve in Fig. 6: a is held fixed near my expected value for Cherenkov readout.

4 π/p

In Paper I we observed that $f^0_{\rm em} \equiv \langle f_{\rm em}(E) \rangle$ is larger for an incident charged pion than for an incident proton (or neutron). This is a consequence of the fact that a leading hadron, carrying a large fraction of the energy, is likely to have the same quark number as the incident hadron. If the collision is instigated by a $\pi^\pm$, there is high probability that the leading hadron is a π^0, but for an incident proton or neutron the leading hadron is most likely a baryon. The mean em fraction $f^0_{\rm em}$ is thus larger for an incident pion than for an incident baryon.

We also observed that for a given material or fine-sampling calorimeter, there is an energy-independent spectrum of hadrons below the incident hadron's energy, and that most energy deposit is by very low-energy particles. This

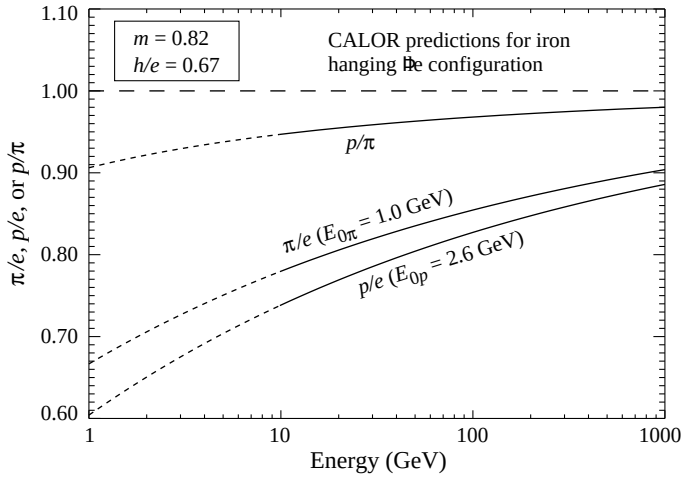

Fig. 7. Expected π/p for one of the SDC reconfigurable absorber test-beam configurations [24] in which $h/e \approx 0.67$. m, $E_{0\pi}$, and E_{0p} are from the fits shown in Fig. 11 of Paper I. pi_p

means that the hadronic response (within a scale factor) of the calorimeter is the same for protons as for pions; h/e is unchanged. The various simulations in that paper found $E_{0\pi} \approx 1$ GeV, with some change from material to material. For protons the Monte Carlo simulations yielded $E_{p0} \approx 2.6$ GeV. This is consistent with the original expectation that E_0 was the approximate multiple-pion threshold[2]. The Z-dependent exponent m for a given material was the same, within statistics, for both p and π^-.

If the exponent m in the powerlaw were less for protons than for pions, then at some energy the sign of the response difference would change, which can be ruled out on physical grounds. Simulations are consistent with equality, which implies that the ratio of the mean hadronic fractions, $f_\pi^0(E)/f_p^0(E)$, is independent of energy. In the powerlaw approximation the scale energy is different for the two cases: $f_p^0/f_\pi^0 = (E_{0p}/E_{0\pi})^{1-m}$. The simulations shown in Paper I, Fig. 11 suggest $f_\pi^0/f_p^0 \approx (2.6/1.0)^{1-m} = 0.83$ for $m = 0.815$ and $f_p^0/f_\pi^0 = 0.87$ for $m = 0.85$.

Thus if $h/e \neq 1$, a calorimeter should give a different response for charged pions than for protons. In the usual case, where $h/e < 1$, pions give the larger response. The effect is illustrated in Fig. 7, where as an example we use $h/e = 0.67$, obtained from CALOR simulations (Paper I, Table 1) for the "iron" configuration of the SDC test-beam calorimeter[24]. It is regrettable that there was not time to measure the effect there.

Since then, the CMS forward calorimeter group at CERN has measured the π/p difference using a calorimeter consisting of quartz fibers embedded in a copper matrix (QFCAL)[13,14]. In this calorimeter, Cherenkov light was detected, most of it coming from em showers, so that h/e was very small, and

Table 2
Calculation of f_p^0/f_π^0 as a function of incident hadron energy (last column) using Eq. (8) and data from Table 2 of Akchurin et al.[14]. $\left\langle f_p^0/f_\pi^0 \right\rangle = 0.859 \pm 0.004$, with $\chi^2 = 13.2$. Most of χ^2 is contributed by the first and third points.

Energy	Response[14]		f_p^0/f_π^0
(GeV)	p/e	π/e	
200	0.562 ± 0.013	0.647 ± 0.001	0.806 ± 0.024
250	0.580 ± 0.010	0.648 ± 0.001	0.838 ± 0.020
300	0.590 ± 0.006	0.658 ± 0.001	0.834 ± 0.012
325	0.592 ± 0.006	0.652 ± 0.001	0.853 ± 0.013
350	$0.607^{+0.001}_{-0.004}$	0.659 ± 0.001	0.868 ± 0.007
375	$0.611^{+0.001}_{-0.003}$	0.664 ± 0.001	0.864 ± 0.005

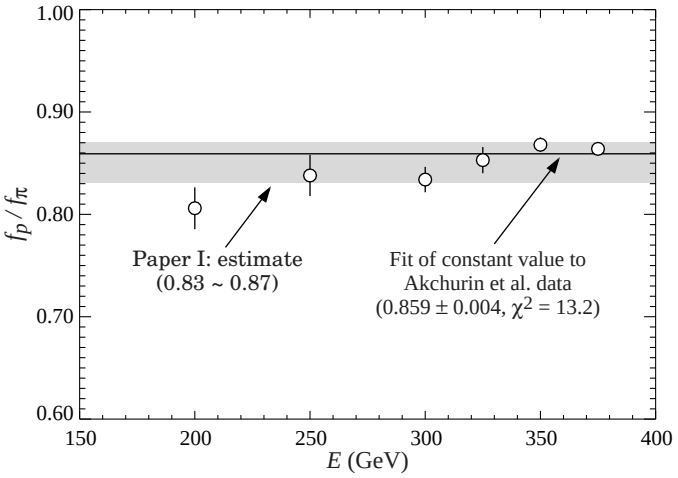

Fig. 8. f_p^0/f_π^0 as calculated from the copper/quartz-fiber calorimeter data of Ref. [14]. The gray band is the range expected from Paper I. wigmans_pi_p

the π–p response difference was maximal. π/e and p/e as a function of energy are reported in Table 2 of Ref. [14] and copied to our Table 2.

Eqation (5) may be rewritten for the pion and proton cases:

$$\begin{aligned} p/e &= 1 - (1 - h/e) f_p^0 \\ \pi/e &= 1 - (1 - h/e) f_\pi^0 \end{aligned} \tag{7}$$

Rearrangement gives us the energy-independent ratio of the mean hadronic

fractions: [6]

$$f_p^0/f_\pi^0 = \frac{1-p/e}{1-\pi/e} \tag{8}$$

The constant ratio, which does not depend upon a powerlaw or any other model for f_h^0, is independent of the detection efficiency factors h and e, as it must be, but the statistical sensitivity is maximal for small h/e. This ratio is calculated in the right column of Table 2 for the Akchurin et al. data. These data together with estimates of the Paper I and a least square fit to a constant f_π^0/f_p^0 are shown in Fig. 8. There is some evidence of energy dependence, but I am inclined not to take it seriously because (a) it does not make theoretical sense, and (b) the authors made a difficult subtraction of π^+ contamination in their positive beam. The contamination was minimal at the highest energy, as is reflected in the uncertainties. If the pion contamination correction were overdone, we would obtain the observed low values at the lower energies. I am probably safe in concluding that $f_p^0/f_\pi^0 \approx 0.86$ for this calorimeter.

In the case of incident kaons, the leading hadron is probably a strange meson, but sometimes a pion. It is unlikely to be a proton or neutron. The response difference between incident pions and kaons should thus be small.

5 *mips*

As indicated above and in Fig. 1, e and h are the efficiencies with which electromagnetic and hadronic energy are converted to visible signal. It is conventional to scale signal sizes, in ADC counts, to the mean response for minimum ionizing particles (*mips*), thus giving them something of an absolute meaning. In practice the "average" signal from penetrating muons, corrected for radiative losses, is assumed to be described by the Bethe-Bloch equation including the density effect. It is then scaled to the value at minimum ionization, presumably defining the *mip*.

But the *mip* is commonly used incorrectly.

In a simplification of the normal derivation of the Bethe-Bloch formula, [7] ionization and excitation energy losses are calculated separately for (soft) distant collisions (low energy transfer per interaction) and (hard) near collisions (high energy transfer). The regions are distinguished by the approximations appropriate to each[26–28]. One hopes for an energy at which they meet; this can

[6] This ratio was not calculated in Ref. [13] or [14].
[7] Fano [26] introduces an intermediate energy transfer region.

be something of a problem in high-Z materials. Each contributes a factor $\ln\gamma$ to the behavior at high energies:

(1) As the particle becomes more relativistic, its electric field flattens and becomes more extended. This extension is limited by polarization of the material. This "density effect" asymptotically removes the $\ln\gamma$ factor contributed by the distant-collision region. The "relativistic rise" is still there, but with half the slope[29]. [8]

(2) The kinematic maximum energy which can be transferred in one collision sets the upper limit for hard energy transfer. Its rise with energy is responsible for the other $\ln\gamma$ factor. As the particle energy increases there is more δ-ray production and the so-called "Landau tail" grows and extends. The most probable energy loss, well below minimum ionization in a region dominated by many soft collisions, shows little or no relativistic rise and approaches a "Fermi plateau." This is strictly true and more easily understood for the closely-related truncated mean energy loss discussed below.

    The δ rays are part of energy loss as described by the Bethe-Bloch equation, and must not be confused with muon radiative processes discussed below.

The "Landau distribution"[30] is not especially useful. It obtains for a thin detector assuming a (constant, mass-independent) Rutherford cross section—i.e. neglecting atomic physics. The variance and higher moments are not finite, and the first moment, the mean energy loss, is finite only because of a maximum single-collision energy transfer $T_{\rm max}$. Sixty years later, one can make fewer approximations and take atomic structure into detailed account. Bichsel's approach[31–34] is to find the energy-loss distribution in a film sufficiently thin that a particle has at most one interaction in it. This distribution is then successively convoluted with itself to obtain the energy deposit distribution in a detector element with normal thickness. [9]

Such a result, for one cell of an argon-filled TPC, is shown by the solid line in Fig. 9. The dotted line is the corresponding Landau distribution. The useful descriptors are the full-width at half-maximum (fwhm) and the most probable deposit (Δ_p). For thicker detectors, (fwhm/Δ_p) is smaller, and Δ_p is a larger fraction of the mean ($\langle\Delta\rangle$). The energy-loss distribution for a minimum-ionizing particle in a 640-μm thick silicon detector, for example, has a most probable loss that is about 70% of the mean. For the reasons mentioned above, the mean loss increases with increasing particle energy, while the most prob-

[8] Review of Particle Physics 2006, hereafter RPP06.

[9] In everyday detectors, energy loss by escaping δ-rays or gain from entering δ-rays is small (2% level), so that "energy loss" and "energy deposit" are used somewhat interchangeably.

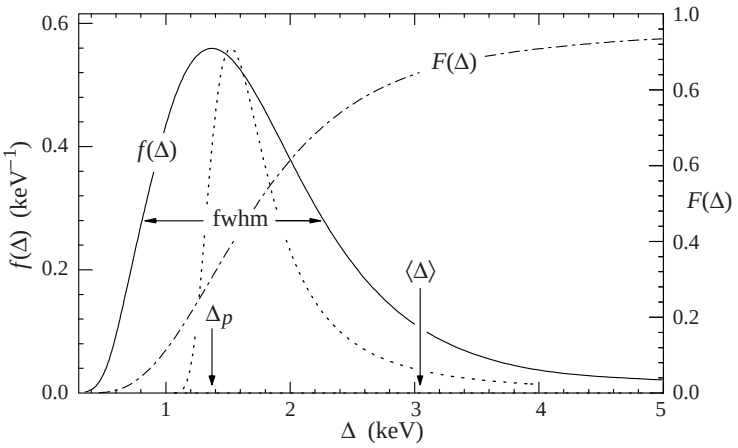

Fig. 9. Energy deposit (Δ) distribution ($f(\Delta)$ by a particle with $\beta\gamma = 3.6$ traversing 1.2 cm of argon gas, adapted from Ref. [34], Fig. 13. The mean energy loss is $\langle\Delta\rangle$ and the most probable energy loss is Δ_p. Solid line: Detailed calculation by Bichsel; dot-dashed line: $F(\Delta) = \int_0^\Delta f(\Delta')d\Delta'$; dashed line: Landau distribution (not normalized). bichsel_fig1

able loss does not change appreciably.

The mean of the energy-loss distribution is ill-defined and ultimately not very useful for describing energy loss by single particles. (It probably finds its best application in dosimetry, where only bulk deposit is of relevance.) The large transfers that contribute to the tail are improbable, making the mean of the experimental distribution subject to large fluctuations and sensitive to cuts and background. This behavior can easily be seen by examining restricted energy loss, i.e. the ionization/excitation Bethe-Bloch $-dE/dx$ calculated with the exclusion of kinetic energy transfer above $T_{\rm cut} < T_{\rm max}$. As a separate matter, the δ-ray spectrum $dN_\delta/dxdT$ can be (a) integrated between $T_{\rm cut}$ and $T_{\rm max}$ to find the number of δ-rays produced per thickness interval x, and (b) multiplied by δ-ray kinetic energy T and integrated over the same interval to find the total energy in the δ-rays, which is identically the truncated tail of the ionization energy loss rate.

Examples for polystyrene scintillator, calculated using RPP06 Eqs. 27.1, 27.2, and 27.5, are shown in Table 3 for several values of $T_{\rm cut}$ at typical test beam muon energies. While the ionization loss rate rises about 17% as the beam energy rises from 10 GeV to 300 GeV, both the number of δ rays and the restricted energy loss rate at a given $T_{\rm cut}$ (here 1, 2, and 5 times the minimum ionization energy) are virtually constant.

Such is the skewness of the distribution that in only 4% of the events is the energy deposit greater than minimum ionization for $x = 1$ g/cm^2. For a more typical 3-mm thick scintillator, with $x = 0.32$ g/cm^2, only 1.3% of the events involve energy deposit greater than minimum ionization. More than five time

minimum ionization is deposited by only 0.26% of the muons, yet these carry 30% of the ionization/excitation energy deposit in the case of a 300 GeV muon. (The reader may verify that the decrease in N_δ with $T_{\rm cut}$ is consistent with the change in $|dE/dx|_{T>T_{\rm cut}}$ in the interval.)

"Restricted energy loss" at best only provides a feel for what is happening. In Bichel's quantitative calculation for a TPC cell shown in Fig. 9, the integral of the distribution is indicated by $F(\Delta)$, where Δ is the actual energy deposit rather than the energy loss rate. Even at minimum ionization, only $\approx 93\%$ of the area is included for $\Delta \lesssim 3.6\Delta_p$. The first moment, or the mean energy, converges to $\langle\Delta\rangle$ much more slowly with increasing cutoff energy; in this example it has reached less than 50% of its actual value with a cutoff of 5 keV. (See Fig. 18 of [34].)

In a sample of a few hundred events, the mean deduced from the data is thus substantially affected by a few rare events with high-energy δ rays. It is very sensitive to the high-energy cut made on the distribution. Most experimental distributions have background which further complicates the determination. A more robust procedure is to fit a limited region around the peak to get an estimator of the most probable loss. As discussed above, this tends to be at about 70% of the theoretical mean at $\beta\gamma \approx 3.5$ for thicker detectors. Figure 27.7 in RPP06 illustrates the situation. More detailed treatments are given by Bichsel[31–34].

In view of the above discussion, it seems likely that the experimental "mean" $\langle\Delta\rangle_{\rm exp}$ is substantially less than $\langle\Delta\rangle$, but in any case $\Delta_p \leq \langle\Delta\rangle_{\rm exp} < \langle\Delta\rangle$. If a paper reports a *mip* calibration via the purported "average" energy deposit, one suspects that the number is low, perhaps as low as 0.7 *mips*.

The ionization/excitation energy fraction sampled by the active region is

$$\text{fraction sampled} = \frac{S\,dE/dx|_{\rm scint}}{S\,dE/dx|_{\rm scint} + A\,dE/dx|_{\rm abs}} \tag{9}$$

where S is the active region thickness, $dE/dx|_{\rm scint}$ is the energy loss rate in the active region (scintillator or other), A is the absorber thickness, and $dE/dx|_{\rm abs}$ is the energy loss rate in the absorber. It is "fairly sampled." This is not the case for electron and muon radiative losses.

Relativistic muons lose energy radiatively by direct pair production, bremsstrahlung, and photonuclear interactions. In iron at 1 TeV, these loss rates are in the ratios 0.58:0.39:0.03. The ratios are fairly insensitive to energy at energies where the radiation is important. The pair:bremsstrahlung ratio is about the same from material to material, while the photonuclear fraction is larger in smaller in materials with smaller atomic mass number. These contributions to

Table 3
Muon ionization/excitation energy loss rate below and above scattered electron kinetic energy $T_{\rm cut}$, and the number of scattered electrons (δ rays) with energy above $T_{\rm cut}$ in polystyrene scintillator. The ionization/excitation energy deposit has a minimum at 1.937 g cm^{-2}MeV^{-1} for muon energy 319 MeV. The number of δ rays with $T > T_{\rm cut}$ is proportional to thickness; for the 3 mm thick tiles in the ATLAS barrel calorimeter $x = 0.32$ g cm^{-2}[35]. Since almost all radiative loss occurs in the iron plates, the radiative part of the energy loss rate is given for Fe in the last row. The units of energy loss are g cm^{-2}MeV^{-1}.

Incident muon energy	10 GeV	30 GeV	100 Ge	300 GeV
$\lvert dE/dx\rvert$ (ionization only)	2.414	2.560	2.702	2.824
$T_{\rm max}$ (GeV)	4.8	22.0	90.2	289.5
$T_{\rm cut} = \lvert dE/dx\rvert_{\rm min}$:				
$\lvert dE/dx\rvert_{T<T_{\rm cut}}$	1.827	1.829	1.829	1.829
$\lvert dE/dx\rvert_{T>T_{\rm cut}}$	0.587	0.731	0.873	0.995
N_δ with $T > T_{\rm cut}$	$0.040x$	$0.041x$	$0.041x$	$0.041x$
$T_{\rm cut} = 2\,\lvert dE/dx\rvert_{\rm min}$:				
$\lvert dE/dx\rvert_{T<T_{\rm cut}}$	1.884	1.886	1.886	1.886
$\lvert dE/dx\rvert_{T>T_{\rm cut}}$	0.530	0.674	0.816	0.938
N_δ with $T > T_{\rm cut}$	$0.020x$	$0.020x$	$0.020x$	$0.020x$
$T_{\rm cut} = 5\,\lvert dE/dx\rvert_{\rm min}$:				
$\lvert dE/dx\rvert_{T<T_{\rm cut}}$	1.960	1.962	1.962	1.962
$\lvert dE/dx\rvert_{T>T_{\rm cut}}$	0.454	0.598	0.740	0.862
N_δ with $T > T_{\rm cut}$	$0.008x$	$0.008x$	$0.008x$	$0.008x$
Radiative part of total $\lvert dE/dx\rvert$ in Fe	0.033	0.133	0.570	1.981

dE/dx rise almost linearly with energy, becoming as important as ionization losses at some "muon critical energy" $E_{\mu c}$: 1183 GeV in plastic scintillator, 347 GeV in iron and 141 GeV in lead. [10] The tables of Lohmann et al.[36] are commonly used. More extensive tables with a somewhat improved treatment of radiative losses are given by Groom et al.[28], and an extension to nearly 300 materials is available on the Particle Data Group web pages[37]. [11]

[10] Other charged particles experience radiative losses as well, but there is no easy mass scaling of the loss rate. In a calorimeter incident pions lose energy by radiation until they interact, but the higher dE/dx is of little consequence and in any case the radiated energy is absorbed.

[11] For the PDG tables, an improvement to the pair-production cross section at high

In equilibrium the muons are accompanied by an entourage of photons and electrons (cascade products from direct pair production and bremsstrahlung) characteristic of radiative losses in the higher-Z absorber. These should be detected with the same efficiency as electrons, although a few high-energy pairs go through the active layers. The procedure for correcting the signal size for the contaminant muon radiative losses is described in many papers, but in particular detail by Åkesson et al. for the HELIOS uranium/scintillator calorimeter[38]. They report $e/mip = 0.70 \pm 0.05$. In correcting for the radiative losses they assumed that the radiative losses were fairly sampled by the scintillator.

The bremsstrahlung is sufficiently continuous as to not introduce significant radiation fluctuations[39], but there are large fluctuations in the pair production energy loss. Monte Carlo calculations by Lanyov[40] indicate that, in absorbers up to typical calorimeter thickness, the most probable energy loss increases only slightly. This is to be expected. Distributions observed in HELIOS[38] and SPACAL[25] demonstrate the broadening, but show more increase of the most probable loss than might be expected.

If the calibration muon beam has been momentum-selected and then travels through air or vacuum to the calorimeter, it enters without its entourage of pairs and bremsstrahlung photons and, until this builds up over several radiation lengths, the signal distribution does not include the full radiation component. If this is desired, there should be a lead brick in the beam.

All of this assumes muons of known energy. "Out of channel" muons, which have gone through or around the test-beam optics, are certainly not dependable calibration particles, but are sometimes used[24]. Cosmic ray muons have a characteristic energy of about 3 GeV, but the flux falls off as about $\cos^2\theta$, where θ is the zenith angle[29]. They can provide a useful for calibration in some situations.

6 e, h, and e/h

Given a credible muon calibration, the quantity e/mip can be measured in an electron beam. In a sampling calorimeter, cascade electrons are predominately produced and absorbed in the inactive higher-Z material, so the signal is significantly smaller than might be expected from the active layer's share of dE/dx ($e/mip \approx 0.6$ to 0.7[41]), but with the uncertainties associated with *most probable* energy deposit vs *average* energy deposit. It can be "tuned"

energies was made which slightly changes the muon dE/dx at high energies in high-Z materials.

by changing the absorber/detector ratio, perhaps to achieve compensation ($h/e = 1$). Other things being equal, the detection efficiency is smaller if the absorber has a higher Z. The critical energy is lower, so characteristic shower electrons are more likely to deposit their energy before leaving the absorber. As a corollary, $e/mip = 1$ for a nonsegmented calorimeter (e.g. an inorganic crystal), and since there is always missing hadronic energy such a calorimeter is always noncompensating.

The hadron efficiency h is more problematical; one finds $a = (1-h/e)E_0^{1-m}$ or an equivalent by fitting the energy dependence of π/e, and assumptions must always be made about the constant multiplier to find h/e and hence h/mip. The multiplier E_0^{1-m} is close to 1 for incident pions, but it is about 20% higher for protons.

h is considerably more difficult to model, but in general it is smaller than e because of the wide variety of ways hadronic energy becomes invisible, e.g. through nuclear binding energy losses and "late" energy deposition (outside the electronics window). [12] It increases somewhat with Z, and can be enhanced by neutron production in uranium. Calorimeters with more "Z-contrast" are more compensating ($e \approx h$) mostly because e is smaller, in spite of the emphasis in the literature on increasing h.

Can we measure h/mip directly? Only by observing hadronic cascades in a calorimeter insensitive to π^0-produced em cascades, or by observing cascades produced by hadrons below the π^0 threshold. In Paper I we speculated about building a calorimeter sensitive only to hadrons (a neutron detector) or to the em sector (a calorimeter sensitive only to Cherenkov radiation), but the context of the discussion was verification of the power approximation for f_h^0 and determination of the power m.

In the spirit of only- (mostly-) em sensitivity in QFCAL, Demianov et al.[42] made preliminary neutron measurements using Bonner spheres[43] adjacent to the QFCAL quartz-fiber calorimeter[13]. The longitudinal and transverse distributions were measured. The results were in fair to good agreement with MARS'96[44] calculations, but not sufficiently detailed to obtain h/mip (or n/mip). Preliminary proposals[45] (in connection with International Linear Collider (ILC) detector R&D) are being made to measure the neutron flux by a variety of methods; future test-beam results will be of great interest.

One might use hadrons with energies below the π^0 threshold. The ZEUS collaboration made measurements with low-energy protons and charged pions with a compensated U/scintillator calorimeter[46]. Interestingly, as the kinetic energy of the beam was decreased from about 5 GeV to about 0.4 GeV, e/h decreased from its high-energy value (one) to the e/mip measured for electrons.

[12] A particularly nice discussion is given by Ferrari and Sala[18].

The lower-energy particles tended to lose much or all of their energy by ionization, so that they became indistinguishable from electrons at sufficiently low energies. The resolution also decreased from its hadronic value, approaching the em resolution until at the lowest energies noise became dominant.

A more desirable (or complimentary) approach might be to use an incident beam of low-energy neutrons. Since $E_{0p} \approx 2.6$ GeV, one might expect the π^0 threshold to be about $T \approx 1.6$ GeV. As the energy is scanned downward, a pure hadronic signal should emerge. The response would not be quite the hadronic signal observed from a higher-energy cascade, but this difference can probably be understood. At very least, measurements in a low-energy neutron beam would be interesting. But the real problem is making the test beam.

7 Resolution

The arrows between boxes in Fig. 1 actually indicate the various probability distribution functions (p.d.f.'s) describing fluctuations in each of the steps. A more complete version, Fig. 10, defines these distributions, which are described in more detail in Table A.1. In the simple model considered in this paper, five p.d.f.'s appear.

The potentially detectable energy deposit, or visible energy, is labeled "vis." It usually means ionization, which sometimes sampled directly but more often via scintillators, where the scintillation light is usually detected by photomultipliers. In rare cases Cherenkov light is sampled. The variance associated with the visible energy distribution distribution at fixed E_e, dominated by fluctuations in the total kinetic energy of neutrons, is the *intrinsic* variance.

The label "samp" refers to the additional fluctuations introduced in sampling the visible energy by a readout transducer such as a photomultiplier.

The stochastic processes are defined as follows:

(1) In the cascade initiated by the incident hadron, energy E_e is transferred to the em sector via π^0 production and decay. Because of its different energy dependence, em energy deposited by nuclear gamma rays is not included in my definition of E_e. The p.d.f. $\Pi(E_e)$ was introduced in Sec. 2 to describe its distribution.
(2) The em energy E_e is detectable with some average efficiency e via the ionization produced mostly by low-energy ("terminal") electrons and positrons. The p.d.f. of the em visible energy deposit at fixed E_e is labeled $g_e(E_e^{\rm vis}|E_e)$.
(3) Quite independently, the hadronic component produces a visible signal

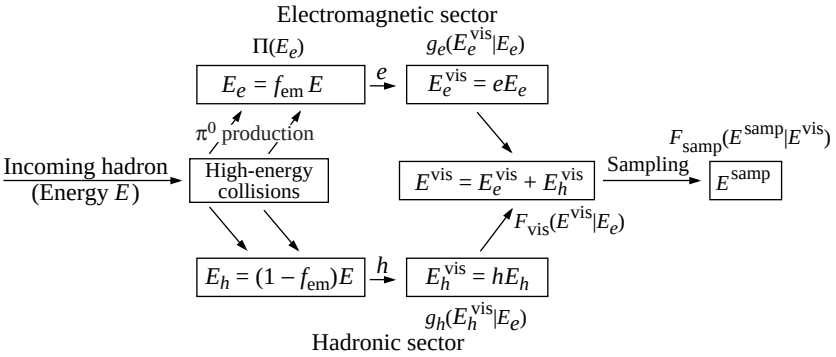

Fig. 10. Energy flow in a calorimeter, with the statistical distributions contributing to the experimental resolution indicated. EFlow_all

via energy loss by charged secondaries. This signal, the result of a variety of mechanisms, is produced with an overall average efficiency h. The visible contribution by nuclear gamma rays is included here. Again, most of the ionization is by low-energy particles. The p.d.f. $g_h(E_h^{\rm vis}|E_e)$ describes the distribution at fixed E_e (E_h).

(4) Only the total deposit $E^{\rm vis} = E_e^{\rm vis} + E_h^{\rm vis}$, with p.d.f. $F_{\rm vis}(E^{\rm vis}|E_e)$, can be sampled. The width of this distribution is identified with the "intrinsic resolution." The product of this distribution with $\Pi(E_e)$, integrated over E_e, is the p.d.f. of the potentially detectable signal, $F_{\rm vis}(E^{\rm vis})$.

(5) Finally, the deposited energy is sampled by measuring the ionization, either directly or by observing scintillation light (Cherenkov light) with photomultipliers or photodiodes. This step is to an extent under the control of the experimenter, since it depends on scintillation efficiency, light collection efficiency, and other design details. For fixed $E^{\rm vis}$ one measures a signal $E^{\rm samp}$, chosen from a distribution $F_{\rm samp}(E^{\rm samp}|E^{\rm vis})$, which is then summed over the intermediate $E^{\rm vis}$ to obtain the final distribution of the signal, $E^{\rm samp}$. Even this step is not a simple convolution, since the variance of $F_{\rm samp}(E^{\rm samp}|E^{\rm vis})$ is proportional to $E^{\rm vis}$, not E.

The intrinsic and sampling distributions were separated in a classic experiment by Drews et al.[47], who used two compensating sandwich calorimeters with scintillator readout with lead and uranium plates, respectively. Alternate sets of scintillators were read out separately. Sampling variations in the two sets were independent, while intrinsic fluctuations were correlated. These were recovered by adding and subtracting variances.

Calculation of the combined distribution is tedious and not entirely obvious; it is relegated to Appendix A. The result (repeating Eq. (A.21)) is

$$\left(\frac{\sigma_{\rm samp}}{E}\right)^2 = \frac{(\pi/e)\sigma^2_{\rm samp0}}{E} + \left[\frac{f^0_{\rm em}\sigma^2_{e0}}{E} + \frac{f^0_h\sigma^2_{h0}h/e}{E}\right] + (1 - h/e)^2\sigma^2_{nc}\,. \quad (10)$$

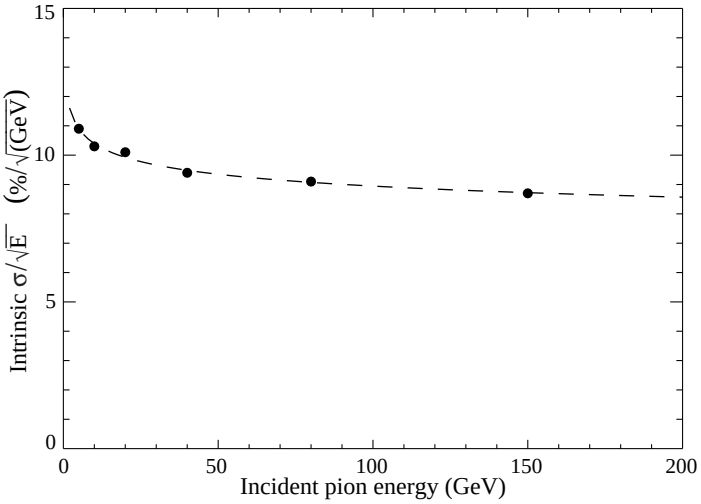

Fig. 11. Wigman's (simulated) data[3] for the intrinsic resolution of a Pb/LAr calorimeter scaled by $1/\sqrt{E}$, fitted with the term in the square brackets of Eq. (10). The fit parameter are given in the text. wigmans_intrinsic

Here $\sigma^2_{\rm samp0}$, σ^2_{e0}, and σ^2_{h0} scale the variances contributed by the sampling, em deposit, and hadronic deposit, respectively. They have the units of energy.

The first term is the familiar sampling contribution, $(C/\sqrt{E})^2$, except that it is multiplied by π/e. This is to be expected *and required*, since this contribution to the variance is proportional to the sampled visible signal, with mean $(\pi/e)E$, rather than to the incident energy E.

The two terms in the square brackets are the two pieces of the intrinsic variance. Even if $h/e = 1$, the intrinsic variance has some energy dependence, since $f_{\bf em}$ increases with energy and f_h increases with energy.

Wigmans[3] has noted that $\sigma_{\rm intr}/\sqrt{E}$ for the simulated lead/LAr calorimeter described in his Table 3.4 decreases with energy, reflecting the gradually increasing transfer of energy to the em sector. His calculated results for six energies, given in his Table 4.3, are plotted in Fig. 11. The curve was obtained by adjusting the intrinsic variance scales σ^2_{e0} and σ^2_{h0}. The best-fit parameters are $\sigma_{e0} = 5.1\%$ and $\sigma_{h0} = 13.7\%$. The fit is remarkably good, and, as expected, σ_{h0} is considerably larger than σ_{e0}.

The last term is the expected "constant term," nearly (but not quite) constant because the fractional variance of $\Pi(E_e)$, σ^2_{nc}, is nearly energy independent, as discussed in Sec. 2. Here I treat it as a constant. It has larger values in calorimeters with higher-Z absorber.

The em part of the intrinsic variance increases in importance as E increases, as does the sampling variance. Both curve downward if plotted vs $1/E$, as shown in Fig. 12. Since the hadronic intrinsic contribution decreases faster

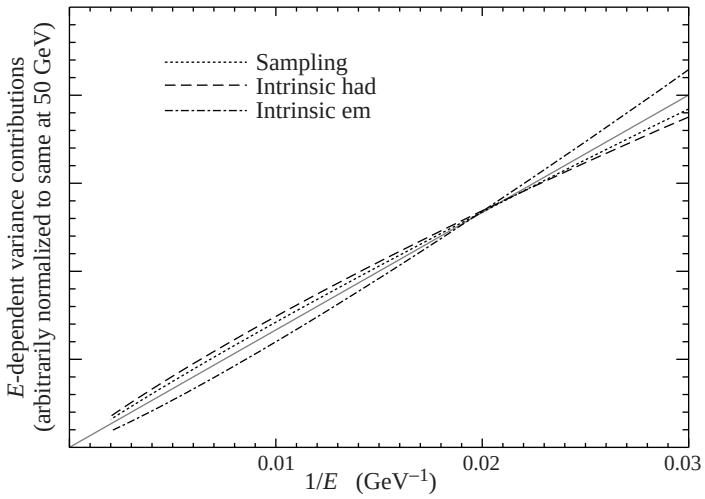

Fig. 12. Shapes of contributions to sampling and intrinsic variance. As $1/E \to 0$, the slopes of the sampling and intrinsic em contributions approach finite constants, since $\pi/e \to 1$ and $f_{\rm em} \to 1$, while the slope of the intrinsic hadronic contribution approaches zero ($f_h \to 0$). groom_res_shape

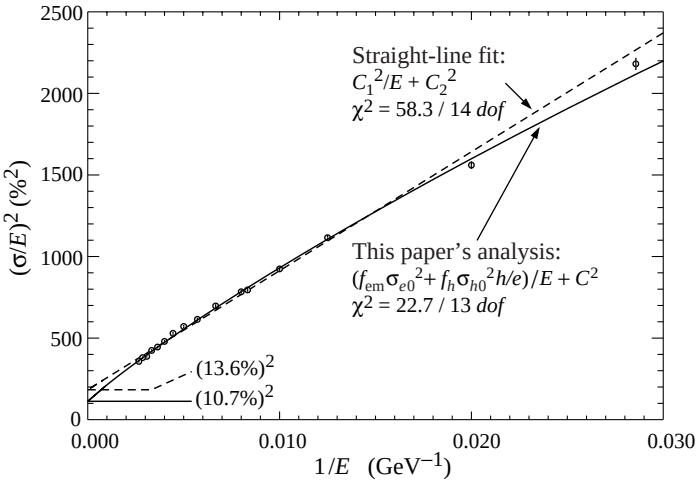

Fig. 13. "Conventional" and Eq. (10) fits to the QFCAL energy response data given in Table 3 of Ref. [13]. The fit parameters are given in Table 4. groom_res_plot

than $1/E$, it curves upward.

It is difficult to verify Eq. (10), even with robust experimental data. The expected resolution should be a linear combination of the three curves shown in Fig. 12 (plus a constant term), so any deviation of the variance from the traditional C_1^2/E will show up as a slight curvature. Moreover, the sampling and em contributions have such similar energy dependence that a simultaneous fit to $\sigma_{\rm samp0}$ and σ_{e0} can be indeterminate.

The square of the fractional energy resolution in QFCAL for incident pions (Akchurin et al.[13], Table 3) is plotted as a function of $1/E$ in Fig. 13. The

Table 4
Parameters for the two fits shown in Fig. 13. The power-law parameters $m = 0.833$, $a = 0.753$ and $h/e = 0.247$ (for $E_0 = 1.0$) from Table 1 were used in the reduction.

$\sigma/E = C_1/\sqrt{E} \oplus C_2$		Eq. (10) with $\sigma_{\rm samp0} = 0$	
Parameter	Value	Parameter	Value
		σ_{e0}	377%
C_1	270%	σ_{h0}	216%
C_2	13.6%	C	10.7%
$C_2/(1-h/e)$	18.0%	$C/(1-h/e)$	14.2%
χ^2/dof	58.3/14	χ^2/dof	22.7/13

data curve downward relative to the "conventional" linear fit, $C_1^2/E + C_2^2$, shown by the dashed line. For QFCAL intrinsic fluctuations were more important than sampling fluctuations except at the lowest energies, although sampling fluctuations were not negligible. Because of the near-degeneracy of sampling and intrinsic em fluctuations, I set $\sigma_{\rm samp0} = 0$ in making a fit, which is shown by the solid curve in the Figure. It describes the data well, and the physics responsible for the curvature is understood.

Parameters for both cases are shown in Table 4. The fittted values for σ_{e0} and σ_{h0} are very much larger than for the example discussed above and shown in Fig. 11; this follows from the excellent resolution of Wigman's model calorimeter and the poor resolution of QFCAL.

Other examples testing the $1/E$ are difficult to find. Many test-beam results are at low energy, many have large errors, and many of the earlier results are presented as functions of $C_1/\sqrt{E} + C_2$ rather than $C_1/\sqrt{E} \oplus C_2$. It will be of interest to test Eq. (10) against further experimental results.

8 Jets

How is calorimeter's response to a jet different than its response to a single pion? There are three situations to consider:

(1) An incident pion. The primary collision usually occurs about an interaction length into the calorimeter. There is a minimum of backscatter ("albedo"). The fragmentation process is dependent on energy and the nuclear environment.

(2) A "test-beam jet," in which trigger counters ensure that the primary interaction occurs in a thin absorber in front of the calorimeter. This is exactly the same as the incident pion case, except for increased albedo because of the high probability that some of the first-collision debris interacts near the front of the calorimeter.
(3) A primary fragmentation jet. The only evident differences from the above cases are the (much) higher energies and a simpler environment; except in heavy-ion collisions just two particles interact. This section concerns whether the mix and distribution of photons, pions, and other particles results in calorimeter response different than the response to a pion or "test-beam jet."

As elsewhere in this paper, the situation is highly idealized: The homogenous or fine-sampling calorimeter is large enough to contain the entire cascade and the structure is uniform throughout. The realities of jet-finding and isolation algorithms, albedo, the effects of the magnetic field, passive material in front of the calorimeter, etc., are all ignored.

The power law approximation for f_h developed in Paper I will be used throughout this section.

A jet with energy E_J consists of photons, mostly from π^0 decay, and "stable" hadrons. (Energy which might be carried away by leptons is ignored.) Since most of the incident "stable" hadron flux consists of charged pions, $E_0 \approx 1$ GeV and $(1 - h/e) \approx a$.

One needs only to sum the calorimeter response to all of these particles to obtain the response to a jet. If R_{ej} is the response to the jth $\pi^0\,(\gamma)$ in the jet (with energy $E_{\pi^0 j}$) and R_{hk} the response to the kth stable hadron (with energy E_{hk}), then the response to a jet is given by

$$E_J^{\rm vis} = \sum_{\rm photons} R_{ej} + \sum_{k=1}^{N_{\rm had}} R_{hk} \ . \tag{11}$$

Using Eqns. (3)–(6) to evaluate R_{hk} and R_{ej}, this reduces to

$$E_J^{\rm vis} = eE_J\Big[1 - a\,E_J^{m-1} \sum_{k=1}^{N_{\rm had}} (E_{hk}/E_J)^m\Big] \ . \tag{12}$$

Alternatively, the spectrum of stable hadrons can be described by a fragmentation function $D(z)$, where z is the hadron's momentum parallel to the jet direction, scaled by the jet's momentum. In the present study z is treated as the fractional energy, i.e. $z \approx E_{\rm had}/E_J$. When the arguments leading to

Eqn. 12 are repeated, one obtains

$$E_J^{\rm vis} = eE_J\Big[1 - a\,E_J^{m-1}\int_0^1 z^m D(z)dz\Big]\ , \tag{13}$$

where $D(z)$ describes the spectrum of all hadrons except for the π^0's.

The sum (Eqn. 12) or integral (Eqn. 13) thus appears as a correction factor to the normal hadronic response of a calorimeter. *If it is unity, the response to a jet is the same as the response to a pion.* In any case it is multiplied by a, which is usually < 0.3. The distinction between a single pion and a jet vanishes as the calorimeter becomes more compensated—except, of course, for the albedo, magnetic field, passive material in front of the calorimeter, and cone-cut effects mentioned above.

If the sum or integral is evaluated for $m = 0$, the mean stable hadron multiplicity $\langle N_{\rm had}\rangle$ is obtained. If $m = 1$, the result is the mean nonelectromagnetic fraction of the jet's energy $\langle F_{\rm had}\rangle$. The desired summation or integral, with $m \approx 0.82$–0.86, is in some sense an interpolation between the two.

In using either experimental or Monte Carlo distributions to evaluate the sum or integral, special treatment of the very low-z region is necessary, as is normalization to an appropriate $\langle F_{\rm had}\rangle$.

The integral in Eqn. 13 is evaluated for four representative cases:

Two experimental results, both with jet energies at or near $M_Z/2$. Since the measurements are for *charged* hadrons, the distributions must be renormalized to include the contributions of such particles as Λ's and K_L's.

(1) Jets from Z decay, as measured by the DELPHI collaboration at LEP[48]. The published fragmentation function is for the entire event, so the function has been normalized downward by a factor of two to describe the individual jets. Data were read from their Fig. 3(b) and extrapolated to $z = 0$.
(2) CDF charged fragmentation function at $\sqrt{s} = 1800$ GeV[49]. $zdN_{\rm ch}/dz$ was extrapolated to $z = 0$ to force $\langle F_{\rm ch}\rangle = 0.65$, their reported value. (Since some of the energy is carried by neutrals, this value is probably too high for consistency with isospin conservation.)

Two samples of TWOJET ISAJET[50] events at $\sqrt{s} = 40$ TeV.[13] In both cases, all hadrons other than π^0's are used:

[13] I am indebted to my SDC collaborator E. M. Wang for running these simulations. This work was jointly reported in Refs. [6] and [7].

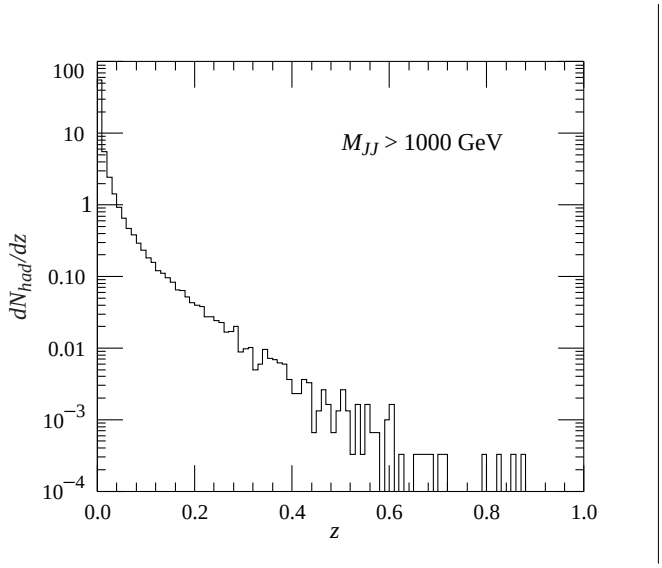

Fig. 14. Distribution in z for ISAJET TWOJET events at $\sqrt{s} = 40$ TeV, for 1000 GeV $< M_{JJ} <$ 2000 GeV. dnhdz1000

(3) 3226 events with p_t (hard scatter) > 40 GeV/c, and (100 GeV $< M_{JJ} <$ 200 GeV). The mean jet momentum is 73 GeV/c, and the mean non-π^0 hadronic multiplicity is 26.

(4) 3042 events with p_t (hard scatter) > 400 GeV/c, and 1000 GeV $< M_{JJ} <$ 2000 GeV. The mean jet momentum is 677 GeV/c, and the mean non-π^0 hadronic multiplicity is 70. The z distribution for these events is shown in Fig. fig:dnhdz1000.

The results are summarized in Table 5. There is ambiguity because of uncertainty in $\langle F_{\rm had}\rangle$ in the simulations and $\langle F_{\rm ch}\rangle$ in the experimental results. If pion production dominates, one might expect $\langle F_{\rm had}\rangle \approx 2/3$ from isospin considerations. (In Paper I, we reported fractions closer to 3/4.) Some of the bias can probably be removed by normalizing $\int zD(z)dz$ to 2/3, as indicated by the table entries in parentheses. As can be seen, the integral is slightly less than unity for the similar low-energy LEP and Tevatron fragmentation functions, and it is slightly greater than unity for simulated 40 TeV jets. Values lie between 0.84 and 1.15 before normalization, and 0.92 to 1.06 after normalization—probably well within the uncertainty of the fragmentation functions in either the experimental or Monte Carlo cases. The integrals also change by about 0.05 if m is changed by 0.01, introducing an additional uncertainty which could be as great as 20%. Given the various uncertainties, I conclude that the correction factor for fragmentation jets at the highest-energy colliders should be between 0.85 and 1.15.

The compensation factor $a \approx (1 - h/e)$ appearing in Eq. (12) and 13 serves to further reduce the effect of the correction factor in producing a jet/π difference. The percentage errors for the two limiting cases 0.85 and 1.15 are plotted

Table 5
Integrals over representative fragmentation functions. Numbers in parentheses are calculated for the nonelectromagnetic energy fraction normalized to 0.67. In the case of the DELPHI and CDF results, the unrenormalized energy fraction is for charged hadrons only.

Source	Process	$\int_0^1 D(z)dz$	$\int_0^1 z^{0.86}D(z)dz$	$\int_0^1 zD(z)dz$
DELPHI	$Z \to jet\ jet$	11.0(12.1)	0.84(0.92)	0.61(0.67)
CDF	$\sqrt{s} = 1.8$ TeV	17.8*(19.9)	0.94(0.97)	0.65(0.67)
ISAJET	40 TeV, $\langle p_J \rangle = 73\,\mathrm{GeV}/c$	26.2(25.2)	1.04(1.00)	0.69(0.67)
ISAJET	40 TeV, $\langle p_J \rangle = 677\,\mathrm{GeV}/c$	69.8(64.7)	1.15(1.06)	0.72(0.67)

* The extrapolated low-momentum part of the function contributes 10 to this total.

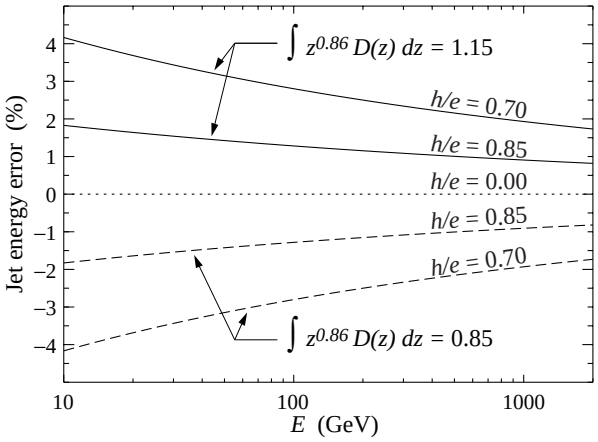

Fig. 15. Energy determination error as a function of jet energy for representative values of h/e, for the two extreme case of the correction factor: 0.85 (top curves, for hard, low-multiplicity jets) and 1.15 (bottom curves, for soft, high-multiplicity jets). jeterror2

in Fig. 15 for calorimeters with $h/e = 0.70$ and $h/e = 0.85$, values which might occur for a Pb/LAr or badly designed metal/scintillator calorimeter. The uncertainty in the exponent m could introduce an error of about 3% for jets below 100 GeV in a poor calorimeter.

In summary: In the context of a power law approximation to the hadronic fraction for an incident pion, the response for an incident jet reduces to a simple correction factor, an integral over the fragmentation function. Given the uncertainties involved, no difference between jet and pion response can be found.

9 Beating the devil

An estimation of the em content of individual events would permit correction for intrinsic fluctuations (reduction of the "constant term"), along with its contribution to energy uncertainty.

Several attempts have been made to use the radial and longitudinal detail to estimate, and correct for, the em cascades. During tests for the SDC construction, it was proposed that the em contribution might come "early" in the cascade, and could be estimated by excess energy deposit in the first layers. This turned out not to be true[51]. The ATLAS barrel calorimeter group adjusts downward the contribution of readout cells with large signals, since these tended to be from em cascades. In the test-beam runs they achieved slight improvements, e.g. from $(46.9 \pm 1.2)\%/\sqrt{E}$ to $(45.2 \pm 2.2)\%/\sqrt{E}$[35]. Ferrari and Sala have simulated such corrections for the LAr TPC ICARUS detector, where very detailed 3D imaging is possible, and conclude that the em content can be fairly well determined from the direct observation of the em cascades[18]. The success of these corrections depends on the detail available, and any gains are usually marginal.

It was long suggested by Mockett[52] that information from a dual-readout calorimeter with different h/e's in the two channels could be used to estimate the electromagnetic fraction $f_{\rm em}$ for each event. Winn[53] has proposed using "orange" scintillator, observing the ionization contribution through an orange filter and observing the Cherenkov contribution through a blue filter. This has not yet been implemented, and looks problematical.

The idea of using a quartz fiber/scintillator fiber calorimeter to extract an estimate of E_e for each event was discussed by Wigmans in 1997[54]. Since then, the DREAM collaboration (Akchurin et al.[55]) has elegantly demonstrated the efficacy of the dual-readout technique, using a copper/optical fiber test-beam calorimeter. It consists of copper tubes, each containing three plastic scintillator fibers and four undoped fibers which produce only Cherenkov light. These are read out separately for each event.

The principle is illustrated in Fig. 16. Akchurin et al.'s notation is used: S for the scintillator signal and Q for the Cherenkov signal, with both energy scales calibrated with electrons. For this example their values $h/e|_S = 0.7$ and $h/e|_Q = 0.2$ are used for the scintillator and nominal Cherenkov readouts respectively. For infinitely good resolution. events with different $f_{\rm em}$ should lie along the solid line drawn from $f_h = 1$ to $f_h = 0$ ($f_{\rm em} = 0$ to $f_{\rm em} = 1$):

$$S = E(f_{\rm em} + f_h(h/e|_S)) \ , \ \text{and} \ \ Q = E(f_{\rm em} + f_h(h/e|_Q)) \ . \tag{14}$$

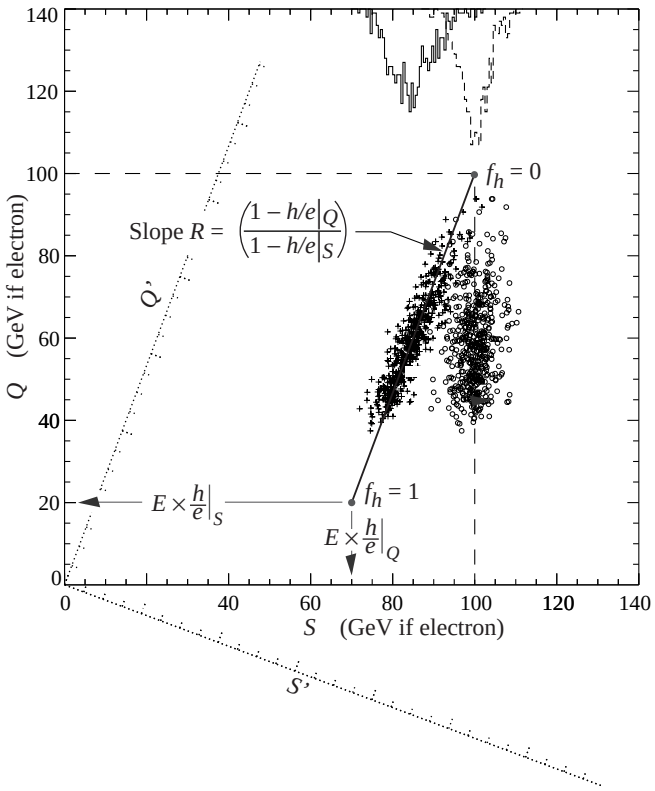

Fig. 16. A toy model showing energy correction for 100 GeV pions in an idealized DREAM calorimeter, where Q is the response in the quartz-fiber readout and S is the response in the scintillator-fiber readout. The observed "events" are shown by the +'s, and the corrected events by the ∘'s. Rotating to a frame in which the Q' axis is parallel to the event locus provides an equivalent reduction. q_vs_sprime

The effects of finite resolution are illustrated using simulations which give $f_{\rm em}$ for 100 GeV negative pions axially incident on a very large lead cylinder. (Results at 30 GeV from the same study are shown in Fig. 3(a).) For this cartoon example I arbitrarily introduced a Gaussian scatter in both $E_{\rm em}$ ($\sigma_{\rm em}/\sqrt{100\ {\rm GeV}} = 1.5\%$) and E_h ($\sigma_h/\sqrt{100\ {\rm GeV}} = 3.0\%$). The "events" are shown by the small +'s in the figure. The solid histogram at the top shows the marginal distribution in S. The mean is 84.7 GeV, the fractional standard deviation is 5.3%, and there is the usual skewness toward high energies.

Energy correction is straightforward. With the definition

$$R = \frac{1 - h/e|_Q}{1 - h/e|_S} \ , \tag{15}$$

Eq. (14) can be solved to obtain

$$E_{\rm corr} = \frac{RS - Q}{R - 1} \ . \tag{16}$$

The circles in Fig. 16 show the same events after reduction via Eq. (16), and the dashed histogram shows the marginal distribution. The mean is 100.1 GeV, the fractional standard deviation is 3.4%, and there is no evident skewness. Complete compensation has been achieved by using the simultaneous readouts.

Alternatively, a coordinate rotation to axes (Q', S') can be made, such that the new Q' axis is parallel to the event locus. The projection of the event distribution onto the new S' axis is of minimal width. Scaled upward by the geometrical factor, it becomes the corrected distribution given by Eq. (16).

The importance of a large "compensation asymmetry" is evident. If the standard deviation in Q is σ_Q and the standard deviation in S is σ_S (both in GeV), then the uncertainty in $E_{\rm corr}$ is approximately

$$\sigma^2_{\rm Ecorr} = \left(\frac{R}{R-1}\right)^2 \sigma^2_S + \left(\frac{1}{R-1}\right)^2 \sigma^2_Q \qquad (17)$$

Since R can be well determined either from test-beam measurements of π/e as a function of energy or from fits to the slope in a plot of Q vs S at one energy, the error in R has been neglected in writing Eq. (17). In the present example $R = (1 - 0.2)(1 - 0.7) = 2.66$, so $\sigma^2_E = 3.20\sigma^2_S + 0.36\sigma^2_Q$. Given the Cherenkov readout, σ^2_Q is likely to be much larger than σ^2_S. The price of the correction is an increased error on each event, but it is clear from Fig. 16 that there is compensating improvement.

DREAM has demonstrated how to detect and remove the effects of fluctuations, albeit with a doubling of the usual number of photomultipliers. Preliminary designs for a full-scale detector are being developed in the context of International Linear Collider (ILC) detector studies[45]. If neutron detection can be added, then the in-principle 1% hadron calorimeter ultimate resolution[54] might be approached.

Alternate schemes simpler than DREAM would be desirable. Winn's scheme[53], taking advantage of the different colors of Cherenkov and (red) scintillation light, uses common detectors but still needs the doubled number of photomultipliers. Clean separation of the two signals would likely be difficult. LSND[56] used a weak scintillator and distinguished between directional Cherenkov light and isotropic scintillation light. But this was a very different kind of detector, a homogenous low-Z detector used in a search for rare signals involving single, low-energy electrons. The electrons at the end of a high-energy shower do not remember the original direction.

10 Discussion

The conceptual picture of the physics of a hadronic cascade and the scaling law it implies have been rich in consequences for understanding the behavior of a hadron calorimeter. The response ratio π/e is particularly simple, and the pion-proton response difference, in retrospect so obvious, was an unexpected surprise. If the incident hadron is a jet rather than a pion, the response is still given by Eq. (4), except that f_h is multiplied by an integral over the fragmentation function which appears to be near unity. Resolution is described by considering in detail the various stochastic processes involved in a hadronic cascade. They cannot be simply convoluted.

Acknowledgments

I am indebted to a large fraction of my calorimetry and radiation physics friends for profitable discussions in the course of formulating these ideas, but particularly so to Richard Wigmans and my collaborators on Paper I: Tony Gabriel, P.K. Job, Nikolai Mokhov, and Graham Stevenson. Conversations with and input from Hans Bichsel, Alberto Fassó, Alfredo Farrari, and John Hauptman have been particularly welcome and useful.

This work was supported by the U. S. Department of Energy under Contract No. DE-AC03-76SF00098.

A Resolution

In the cascade initiated by a hadron with energy E, energy E_e is transferred to the em sector via π^0 production and decay. The energy deposit in the resulting em cascades produce ionization with some efficiency e. Most of the ionization is via energy loss by the abundant low-energy electrons. In the case of the CMS Cu/quartz test calorimeter[13], Cherenkov light samples the electron path length. Quite independently, the hadronic component produces ionization through the many mechanisms involved in hadronic cascades, again mostly by ionization by low-energy particles, with overall efficiency h. Each goes its stochastic way independently of the other. One must calculate the distribution of the sum of the contributions to the ionization with the constraint that E_e is fixed, then integrate over E_e. Finally, the distribution is "sampled" by directly collection ions or detecting scintillation light (or Cherenkov light) via photomultipliers or phodiodes, The resulting probability distribution function

(p.d.f.) has a variance somewhat different than the usual $(\sigma/E) = \sigma'/\sqrt{E} \oplus \sigma_{\rm const}$. The differences, discussed in Sec. 7, are easily understood physically.

To expedite the calculations, it is useful to associate a characteristic function $\langle e^{iux} \rangle = \phi(u)$ (c.f.) with each p.d.f. $f(x)$. It is essentially the Fourier transform of the p.d.f., and is discussed in the *Probability* section of Ref. [?] and many other places[57]. Among the properties I will use are:

- Convolution of p.d.f.'s becomes multiplication of c.f.'s:

$$f(x) = \int f_1(x) f_2(x-y) dy \quad \Longrightarrow \quad \phi(u) = \phi_1(u)\phi_2(u) \tag{A.1}$$

- Let the conditional p.d.f. of $f_2(x|z)$ be $\phi_2(u|z)$ and the p.d.f. of z be $f_1(z)$. Then

$$\phi(u) = \int f_1(z)\phi_2(u|z) dz \ . \tag{A.2}$$

- If ϕ_2 (above) is of the form $\phi_2(u|z) = A(u)\exp(ig(u)z)$, then

$$\phi(u) = A(u)\phi_1(g(u)) \ . \tag{A.3}$$

  where $\phi_1(u)$ is the c.f. of $f_1(z)$.
- The c.f. of a Gaussian p.d.f. with mean m and variance σ^2 is

$$\phi(u) = \exp\left(imu - \sigma^2 u^2/2\right) \ . \tag{A.4}$$

- Higher moments may be included by continuing the series:

$$\phi(u) = \exp\left(imu - \sigma^2 u^2/2 - i\mu_3 u^3/3!\right) + \ldots \tag{A.5}$$

  Here μ_3 is the third moment of the distribution about the mean. The dimensionless "coefficient of skewness" $\gamma_1 = \mu_3/\sigma^3$ was introduced in Sec. 2 and will be used here.

The arrows between boxes in Fig. (1) actually indicate the various probability distribution functions (p.d.f.'s) describing fluctuations in each of the steps. A more complete version, Fig. 10, defines these distributions, which, along with their c.f.'s, means, and variances are given in Table A.1. The notation is somewhat verbose in the interest of clarity. Throughout the calculations, the primary hadron energy E is implicit and constant. It is also convenient to somewhat interchangeably use $f_e = E_e/E$, $E_h = (E - E_e)$, and $f_h = E_h/E$.

The p.d.f. $\Pi(E_e)$ is discussed in Sec. 2. For reasons discussed there, E_c (or $f_{\rm em}$) is chosen as the independent variable rather than its hadronic counterpart E_h (or f_h). Typical simulations are shown in Figs. 2 and 3. The mean of E_e/E was

Table A.1
Probability distribution functions (p.d.f.'s) and characteristic functions (c.f.'s) used in the resolution discussion. The primary energy E is an implicit conditional variable, and the em energy E_e is the independent conditional variable used in the development. The p.d.f. of the final sampled energy is not used explicitly.

Distribution	p.d.f.	c.f.	Mean	Variance
Energy of π^0's	$\Pi(E_e)$	$\phi_\Pi(u)$	E_e	$E^2\sigma_{nc}^2$
Ionization in em showers	$g_e(E_e^{\rm vis}\|E_e)$	$\phi_{ge}(u\|E_e)$	eE_e	$eE_e\sigma_{e0}^2$
Ionization by hadrons	$g_h(E_h^{\rm vis}\|E_e)$	$\phi_{gh}(u\|E_e)$	$h(E-E_e)$	$h(E-E_e)\sigma_{h0}^2$
Total ionization, fixed E_e	$F_{\rm vis}(E^{\rm vis}\|E_e)$	$\phi_{\rm vis}(u\|E_e)$	Eq. (A.13)	Eq. (A.13)
Total ionization	$F_{\rm vis}(E^{\rm vis})$	$\phi_{\rm vis}(u)$	Eq. (A.15)	Eq. (A.15)
Sampled signal, fixed $E^{\rm vis}$	$F_{\rm samp}(E^{\rm samp}\|E^{\rm vis})$	$\phi_{\rm samp}(u\|E^{\rm vis})$	$E^{\rm samp}-E^{\rm vis}$	$eE^{\rm vis}\sigma_{\rm samp0}^2$
Final sampled signal	$[F_{\rm samp}(E^{\rm samp})]$	$\phi_{\rm samp}(u)$	Eq. (A.20)	Eq. (A.21)

defined as $f_{\rm em}^0$, the fractional variance was found to be σ_{nc}^2 ("nearly constant"), and its coefficient of skewness γ_1 was found to be about 0.6. Its c.f. is thus

$$\phi_\Pi(u) = \exp\left(iuf_{\rm em}^0 E - u^2\sigma_{nc}^2E^2/2 - iu^3\gamma_1\sigma_{nc}^3E^3/3! + \ldots\right) . \tag{A.6}$$

The skewness is carried forward in the calculation. The other p.d.f.'s are assumed to be near-Gaussian, with c.f.'s of the form given in Eq. (A.4).

The conditional p.d.f. $g_e(E_e^{\rm vis}|E_e)$ describes the visible signal produced by the deposit of E_e in the em sector. "Visible" means energy deposit, usually ionization, which can be sampled by an appropriate transducer. Its mean value is eE_e,[14] and its c.f. is $\phi_{ge}(u|E_e)$. The variance for an ensemble of events with the same E_e should be proportional to E_e. The c.f. may be written as

$$\phi_{ge}(u|E_e) = \exp(iueE_e - u^2\sigma_{e0}^2eE_e/2) . \tag{A.7}$$

where σ_{e0}^2 scales the variance. Since the variance has units of (energy)^2 and is proportional to the energy, σ_{e0}^2 has the units of energy.

Similarly, the distribution of ionizing hadronic energy at fixed E_e is given by $g_h(E_h^{\rm vis}|E_e)$. The mean is $h(E-E_e)$. (Since $E_h = E - E_e$, it is sufficient to express the condition on E_h as a condition on E_e.) In analogy to Eq. (A.7), I write the c.f. as

$$\phi_{gh}(u|E_e) = \exp(iuh(E-E_e) - u^2\sigma_{h0}^2h(E-E_e)/2) . \tag{A.8}$$

The complicated hadronic response is dominated by a small number of colli-

[14] The normalization of e and h is ignored because at the end only the ratio h/e appears.

sions with large nuclear binding energy losses, so its distribution is wider than the em response[23,38,58]. It is thus expected that $\sigma_{h0}^2 > \sigma_{e0}^2$, but as shown in Sec. 7 it is hard to distinguish the ways the contributions of σ_{e0}^2 and the sampling term modify the energy dependence of the resolution.

I interpret $g_e(E_e^{\rm vis}|E_e)$ and $g_h(E_h^{\rm vis}|E_e)$ as the em and hadronic contributions, respectively, to the intrinsic resolution. This point will be explored later.

Only the total ionization (or Cherenkov light) $E^{\rm vis} = E_e^{\rm vis} + E_h^{\rm vis}$ can be sampled. Let the conditional p.d.f. of $E^{\rm vis}$ be $F_{\rm vis}(E^{\rm vis}|E_e)$:

$$F_{\rm vis}(E^{\rm vis}|E_e) = \int g_e(E_e^{\rm vis}|E_e)\, g_h(E^{\rm vis} - E_e^{\rm vis}|E_e) dE_e^{\rm vis} \tag{A.9}$$

This integral is a simple convolution, so by Eq. (A.1)

$$\phi_{\rm vis}(u|E_e) = \phi_{ge}(u|E_e)\phi_{gh}(u|E_e)\ . \tag{A.10}$$

The sum over E_e results in the distribution

$$F_{\rm vis}(E^{\rm vis}) = \int \Pi(E_e)\, F_{\rm vis}(E^{\rm vis}|E_e) dE_e\ . \tag{A.11}$$

Via Eq. (A.2) the c.f. of $F_{\rm vis}$ is

$$\phi_{\rm vis}(u) = \int \Pi(E_e)\, \phi_{\rm vis}(u|E_e) dE_e\ . \tag{A.12}$$

The c.f. $\phi_{\rm vis}(u|E_e)$ can be calculated using Eqs. (A.7) and (A.8). For simplicity here and in the algebra leading to Eq. (A.15), it is convenient to define $\Delta\sigma^2 = \sigma_{h0}^2 h/e - \sigma_{e0}^2$. Terms involving E_e are collected into the second exponential:

$$\phi_{\rm vis}(u|E_e) = e^{iuhE - u^2\sigma_{h0}^2 hE/2} \times e^{ieE_e(u(1-h/e) - iu^2\Delta\sigma^2/2)} \tag{A.13}$$

Written in this way, $\phi_{\rm vis}(u|E_e)$ is of the form $A(u)\exp(ig(u)z)$, so by Eq. (A.3),

$$\phi_{\rm vis}(u) = e^{iuhE - u^2\sigma_{h0}^2 hE/2} \times \phi_\Pi(ue(1-h/e) - iu^2 e\Delta\sigma^2/2)\ , \tag{A.14}$$

where $g(u)$ is identified with $e(u(1-h/e) - iu^2\Delta\sigma^2/2)$. $\phi_\Pi(u)$ is given by Eq. (A.6), so it remains to substitute this function into Eq. (A.14) and collect the terms multiplying powers of u. These terms can then be identified as the mean, variance, and skewness of $F_{\rm vis}(E^{\rm vis})$. After considerable algebra, Eq. (A.14) yields

$$\begin{aligned}\phi_{\rm vis}(u) = & \exp\Big(iueE(f^0_{\rm em} + f^0_h h/e) \\ & - \tfrac{1}{2}u^2eE[f_{\rm em}\sigma^2_{e0} + f^0_h\sigma^2_{h0}h/e + (1-h/e)^2\sigma^2_{nc}e^2E^2] \\ & - \tfrac{1}{3!}u^3[\gamma_1\sigma^3_{nc}e^3E^3(1-h/e)^3 + 3\sigma^2_{nc}\Delta\sigma^2e^2E^2(1-h/e)\Big] + \ldots\Big) \end{aligned} \tag{A.15}$$

The final step is to "sample" the ionization with whatever output transducer is being used. Although the experimenter has little control over the variance of $F_{\rm vis}(E^{\rm vis})$.[15] the design might be changed to improve light collection, for example, if the variance contribution due to photoelectron statistics were significant. Again a Gaussian distribution is assumed. The variance contribution from the sampling transducer is proportional to $E^{\rm vis}$:

$$F_{\rm samp}(E^{\rm samp}|E^{\rm vis}) = \frac{1}{\sqrt{2\pi\sigma^2_{\rm samp0}E^{\rm vis}}}\exp\left[-\frac{(E^{\rm samp}-E^{\rm vis})^2}{2\sigma^2_{\rm samp0}E^{\rm vis}}\right] \tag{A.16}$$

$$\phi_{\rm samp}(u|E^{\rm vis}) = \exp[iE^{\rm vis}(u + \tfrac{i}{2}u^2\sigma^2_{\rm samp0})] \tag{A.17}$$

$$\phi_{\rm samp}(u) = \int F_{\rm vis}(E^{\rm vis}|E_e)\phi_{\rm samp}(u|E^{\rm vis})dE^{\rm vis} \tag{A.18}$$

Since the variance is not a constant, a simple convolution is again insufficient. Following the recipe of Eq. (A.3), $g(u) = u + iu^2\sigma^2_{\rm samp0}/2$ is substituted for u in Eq. (A.15):

$$\phi_{\rm samp}(u) = \phi_{\rm vis}(u + \tfrac{iu^2}{2}\sigma^2_{\rm samp0}) \tag{A.19}$$

The mean pion response (the multiplier of iu in Eq. (A.15) is unaffected:

$$\begin{aligned} \text{“}\pi\text{”} = & eE(f^0_{\rm em} + f^0_h h/e)\ ; \\ \text{or}\quad \pi/e = & \ 1 - (1-h/e)f^0_h\ , \end{aligned} \tag{A.20}$$

so that the usual form for π/e (Eq. (4) is recovered.

However, $eE(f^0_{\rm em}+f^0_h h/e)\sigma^2_{\rm samp0}$ is added to the variance of $F_{\rm vis}(E^{\rm vis})$ (the multiplier of $-iu^2/2$ in Eq. (A.15)). The final fractional variance for the calorimeter is

$$\left(\frac{\sigma_{\rm samp}}{E}\right)^2 = \frac{(f^0_{\rm em} + f^0_h h/e)\sigma^2_{\rm samp0}}{E} + \left[\frac{f^0_{\rm em}\sigma^2_{e0}}{E} + \frac{f^0_h\sigma^2_{h0}h/e}{E}\right] + (1-h/e)^2\sigma^2_{nc}$$

[15] There are two caveats here: The effects of noncompensation can be minimized by the methods used by the DREAM collaboration[55], as discussed in Sec. 9 and (in principle so far) by measuring the neutron flux on an event-by-event basis[17] in order to reduce the intrinsic resolution contribution of $g_h(E^{\rm vis}_h|E_e)$.

$$= \frac{(\pi/e)\sigma^2_{\rm samp0}}{E} + \left[\frac{(1-f^0_h)\sigma^2_{e0}}{E} + \frac{f^0_h\sigma^2_{h0}h/e}{E}\right] + (1-h/e)^2\sigma^2_{nc}\ , \quad \text{(A.21)}$$

where I have followed convention and scaled the energy to electron calibration: $eE_e \to E$. This is *almost* the usual form for the resolution ($\sigma/E = C_1/\sqrt{E} \oplus C_2$), but with some important differences:

(1) The first term, the sampling contribution, is scaled by the em response. Since it is the ionization which is sampled, this contribution is perforce proportional to π/e.
(2) The terms in square brackets are the em and hadronic contributions to the intrinsic variance. The shape and interpretation of these terms is discussed in Sec. 7.
(3) The analysis reproduces the familiar "constant term," with variance contribution explicitly proportional to $(1-h/e)^2$. In Sec. (2) it was found it to be only "nearly constant," with a value of about 12.5% [16] at 100 GeV in lead and slowly decreasing with $\ln E$. It was treated as a constant in this development.

The third moment about the mean (μ_3) of the sampled distribution is the coefficient of $-iu^3/3!$ in $\phi_{\rm samp}(u)$:

$$\mu_3 = \gamma_1\sigma^3_{nc}E^3(1-h/e)^3 + 3\sigma^2_{nc}\Delta\sigma^2E^2(1-h/e) + 3E\sigma^2_{\rm vis}\sigma^2_{\rm samp0}\ , \quad \text{(A.22)}$$

where the energy is again scaled to the electron calibration: $eE \to E$. Here $E\sigma^2_{\rm vis}$ is the variance of $F_{\rm vis}(E_{\rm vis})$, the coefficient of $-u^2/2$ in Eq. (A.15).

The first term is to be expected in any noncompensating calorimeter; it is just the skewness of $\Pi(E_e)$ "playing through" to the end. As discussed in Sec. 2, the dimensionless coefficient of skewness, γ_1, is about 0.06 for the model discussed there (π^- on Pb, using an old version of FLUKA), and $\sigma_{nc} = 12.5\%$ at 100 GeV with some mild energy dependence. $\gamma_1\sigma^3_{nc}E^3$ is the actual third moment about the mean of $\Pi(E_e)$.

It is interesting that the visible energy deposition and sampling terms also contribute to the skewness. In the first case, this is because the variance of the visible energy at fixed E_e is proportional to E_e, and so at large E_e a wider distribution is contributed to $F_{\rm vis}(E^{\rm vis})$ than for low E_e—even though for a given E_e the distribution is (taken to be) Gaussian.

For the same reason, sampling also contributes to the skewness. The first two contributions both vanish if $h/e = 1$, but the third term does not. Even in the

[16] This value comes from a particular simulation. The experimental number should be used instead.

case of a compensating calorimeter, we should not expect an exactly Gaussian distribution.

References

[1] T.A. Gabriel, D.E. Groom, P.K. Job, N.V. Mokhov, and G.R. Stevenson, Nucl. Instr. and Meth. A 338 (1994) 336–347. gabriel94

[2] D.E. Groom, Energy scaling of low-energy neutron yield, the e/π ratio, and hadronic response in a calorimeter, Proc. Workshop on Calorimetry for the Superconducting Super Collider, Tuscaloosa, Alabama, 13–17 March 1989, eds., R. Donaldson and M.G.D. Gilchrise, World Scientific, (1990) 59–75. tuscaloosa90

[3] R. Wigmans, *Calorimetry: Energy Measurement in Particle Physics, International Series of Monographs on Physics*, vol. 107, Oxford University Press (2000). wigmansbook

[4] D. E. Groom, Energy Scaling of Low-Energy Neutron Yield, the e/π Ratio, and Hadronic Response in a Calorimeter, Proc. of the ECFA Study Week on Instrumentation Technology for High-Luminosity Hadron Colliders, Barcelona, Spain, 14–21 Sept. 1989, ed. by E. Fernandez and G. Jarlskog, CERN 89-10, 549–550, and ECFA, (1989) 89–124. barcelona89

[5] D. E. Groom, Contributions of Albedo and Noncompensation to Calorimeter Resolution, Proc. of the 1990 DPF Summer Study on High Energy Physics Research Directions for the Decade, Snowmass CO, June 25–July 13, 1990, ed. by E. L. Berger and R. Craven, World Scientific, (1992) 403–406. snowmass90

[6] D. E. Groom and E. M. Wang, Jet Response of a Homogenous Calorimeter, Proc. of the Fort Worth Symposium on Detector R&D for the SSC, Forth Worth TX, 15–18 Oct. 1990, ed. by M. G. D. Gilchriese and V. Kelly, World Scientific (1991) 385–387. fortworth90

[7] D. E. Groom and E. M. Wang, Jet Response of an Ideal Calorimeter, Vol. III, Proc. of the ECFA Large Hadron Collider Workshop, Aachen (4–9 October 1990), CERN 90-10 (1990) 315–319. aachen90

[8] D. E. Groom, Four-Component Approximation to Calorimeter Resolution, Proc. II Inter. Conf. on Calorimetry in High Energy Physics, Capri, Italy, 14–18 October 1991, ed. by A. Ereditato, World Scientific (1992) 376–381. capri91

[9] D. E. Groom, Energy flow in a hadronic cascase: Application to hadron calorimetry (invited talk), Proc. VII Inter. Conf. on Calorimetry in High Energy Physics, Tucson, Arizona, 9–14 November 1997, ed. E. Cheu, T. Embry, J. Rutherfoord, R. Wigmans, World Scientific (1998) 507–521. protoDREAM97

[10] A. Capella, et al., Phys. Rep. 236 (1994) 225. DPM

[11] http://aliceinfo.cern.ch/static/Offline/fluka/manual/ aliceFLUKA

[12] W.R. Nelson, H. Hirayama, and D.W.O. Rogers, The EGS4 Code System, SLAC-265, Stanford Linear Accelerator Center (Dec. 1985). FLUKA now contains its own em radiation transport code; this and other codes have largely supplanted EGS in high-energy physics applications. EGS4

[13] N. Akchurin, et al., Nucl. Instr. and Meth. A 399 (1997) 202. qcal97: QFCAL e, gamma, hadron

[14] N. Akchurin, et al., Nucl. Instr. and Meth. A 408 (1998) 380. wigmans_pi_p98: QFCAL pi/p

[15] R. Wigmans, Ann. Rev. Nucl. Part. Sci. 41 (1991) 133. wigmansAnnRev

[16] C. Leroy and P-G. Rancoita, Rep. Prog. Phys. 63 (2000) 505. leroy00

[17] R. W. Wigmans, Rev. Sci. Instr. 69 (1998) 3723. wigmans98_neut

[18] A. Ferrari and P. R. Sala, Physics processes in hadronic showers (invited talk), Proc. IX Inter. Conf. on Calorimetry in High Energy Phys., Annecy, October 9–14 2000, B. Aubert, J. Colas, P. Nédelec, L. Poggioli eds., Frascati Physics Series, (2001) 31–55. ferrari00

[19] M. De Vincenzi, et al., Nucl. Instr. and Meth. A 243 (1986) 348. wa78

[20] D. Acosta, et al., Nucl. Instr. and Meth. A 308 (1991) 481. spacal91

[21] J. B. Liu, Testbeam results for the CDF endplug hadron calorimeter, Proc. VII Inter. Conf. on Calorimetry in High Energy Physics, Tucson, Arizona, 9–14 November 1997, ed. E. Cheu, T. Embry, J. Rutherfoord, R. Wigmans, World Scientific, (1998) 237–240. jinbo98

[22] J. Behrens, et al., Nucl. Instr. and Meth. A 289 (1990) 115. behrens90

[23] S. Abachi, et al., Nucl. Instr. and Meth. A 324 (1993) 53. D0

[24] A. Beretvas, et al., Nucl. Instr. and Meth. A 329 (1993) 50–61. hangingfile

[25] D. Acosta, et al., Nucl. Instr. and Meth. A 320 (1992) 128. spacal92

[26] U. Fano, Ann. Rev. Nucl. Sci. 13 (1963) 1. fano63

[27] B. Rossi, *High-Energy Particles*, (Prentice-Hall, Inc., Englewood Cliffs, NJ, 1952). rossi52

[28] D. E. Groom, N. V. Mokhov, and S. I. Striganov, Atomic and Nuclear Data Tables 78 (2001) 183. ADNDT01

[29] W.-M. Yao, et al., The Review of Particle Physics, J. Phys. G XXXX (2006) 1. (To be published June 2006; update in proof.) RPP06

[30] L. Landau, J. Phys. VIII (1944) 201.

[31] H. Bichsel, Rev. Mod. Phys. 60 (1988) 663. bichsel88

[32] H. Bichsel, Nuc. Instr. and Meth. B 6 (1990) 136. bichsel90

[33] H. Bichsel, Ch. 87 in the Atomic, Molecular and Optical Physics Handbook, G. W. F. Drake, editor (Am. Inst. Phys. Press, Woodbury NY, 1996). bicheslAMORPH

[34] H. Bichsel, A method to improve tracking and particle identification in TPCs and silicon detectors, Nuc. Instr. and Meth. A (to be published, 2006). bichsel06

[35] F. Ariztizabal, et al., Nucl. Instr. and Meth. A 349 (1994) 384. ATLAScavalli

[36] W. Lohmann, R. Kopp, and R. Voss, Energy loss of muons in the energy range 1–10000 GeV, CERN Report 85-03 (1985). lohmann85

[37] `http://pdg.lbl.gov/AtomicNuclearProperties` AtomicNuclearProperties

[38] T. Åkesson, et al., Nuc. Instr. and Meth. A 262 (1987) 243. akesson87: HELIOS

[39] A. Van Ginneken, Nucl. Instr. and Meth. A 251 (1986) 21. vanginneken86

[40] S. I. Striganov, private communication (2006), using figures from A. V. Lanyov, "Characteristics of muon accompaniment in matter," (in Russian), IFVE-98-145 (June 1989). striganov06

[41] R. Wigmans, Nucl. Instr. and Meth. A 259 (1987) 389. wigmans87

[42] A. Demianov, et al., CMS Internal Note CMS IN 2000/020 (February, 2000). bonnersphere

[43] R. L. Bramblett, R. I Ewing, and T. W. Bonner, Nucl. Instr. and Meth. 9 (1960) 1. bonner60

[44] I. Azhgirey, et al., Nucl. Instr. and Meth. A 408 (1998) 535. MARS96

[45] R. Wigmans et al, "Dual-Readout Calorimetry for High-Quality Energy Measurements", October 2001, proposal to Advanced Detector Research Program of DoE; `http://www.phys.ttu.edu/dream` ILVdual DoE proposal for LHC detector

[46] A. Andreson, et al., Nucl. Instr. and Meth. A 336 (1993) 23. zeus_proton: ZEUS low-energy protons

[47] G. Drews, et al., Nucl. Instr. and Meth. A 290 (1990) 335. drews90

[48] P. Aarnio et al., Phys. Lett. 240B (1990) 271. delphi

[49] F. Abe et al., Phys. Rev. Lett. 65 (1990) 968. CDFjets

[50] F. E. Paige and S. D. Protopopescu, Physics of the Superconducting Supercollider, ed. by R. Donaldson and J. Marx (Snowmass CO, 1986), 320. ISAJET

[51] D. Green, private communication, about 1990. dangreen

[52] P. Mockett, A review of the physics and technology of high-energy calorimeter devices, Proc. 11th SLAC Summer Inst. Part. Phy., July 1983, SLAC Report No. 267 (July 1983). protoDREAM

[53] D. R. Winn and W. A. Worstell, IEEE Trans. Nuc. Sci 36, (1989) 334. winn89

[54] R. Wigmans, Quartz Fibers and the Prospects for Hadron Calorimetry at the 1% Resolution Level, Proc. VII Inter. Conf. on Calorimetry in High Energy Physics, Tucson, Arizona, 9–14 November 1997, ed. E. Cheu, T. Embry, J. Rutherfoord, R. Wigmans, World Scientific, (1998) 182–193. protoDREAM97

[55] N. Akchurin, et al., Nucl. Instr. and Meth. A 537 (2005) 537 DREAM05

[56] C. Athanassopoulos , et. al., Nucl. Instr. and Meth. A 388, (1997) 149–172. LSND: FIND THE DESCRIPTION!

[57] H. Cramér, *Mathematical Methods of Statistics, Princeton Univ. Press*, New Jersey (1958). cramer

[58] U. Behrens, et al., Nucl. Instr. and Meth. A 289 (1990) 115. zeus_FCAL